ROADWAY SAFETY INSTITUTE

Human-centered solutions to advanced roadway safety

Improving Intersection Safety Through Variable Speed Limits for Connected Vehicles

Michael Levin
Rongsheng Chen

Department of Civil, Environmental, and Geo- Engineering
University of Minnesota

Chen-Fu Liao
Department of Mechanical Engineering
University of Minnesota

Tab Zhang
Department of Computer Science and Engineering
University of Minnesota

Final Report

REGION 5

CTS 19-12

University of Minnesota
Driven to Discover

The University of Akron

ILLINOIS
University of Illinois at Urbana-Champaign

Southern Illinois University Edwardsville

Western Michigan University

Technical Report Documentation Page

1. Report No.	2.	3. Recipients Accession No.
CTS 19-12		

4. Title and Subtitle	5. Report Date
Improving intersection safety through variable speed limits for connected vehicles	May 2019
	6.

7. Author(s)	8. Performing Organization Report No.
Michael Levin, Rongsheng Chen, Chen-Fu Liao, Tab Zhang	

9. Performing Organization Name and Address	10. Project/Task/Work Unit No.
Department of Civil, Environmental, and Geo- Engineering University of Minnesota 500 Pillsbury Drive S.E. Minneapolis, MN 55455-0116	CTS #2018055 11. Contract (C) or Grant (G) No. DTRT13-G-UTC35

12. Sponsoring Organization Name and Address	13. Type of Report and Period Covered
Roadway Safety Institute Center for Transportation Studies University of Minnesota University Office Plaza, Suite 440 2221 University Ave SE Minneapolis, MN 55455	Final Report 14. Sponsoring Agency Code

15. Supplementary Notes

http://www.roadwaysafety.umn.edu/publications/

16. Abstract (Limit: 250 words)

Autonomous vehicles create new opportunities for innovative intelligent traffic systems. Variable speed limits, which is a speed management systems that can adjust the speed limit according to traffic condition or predefined speed control algorithm on different road segments, can be better implemented with the cooperation of autonomous vehicles. These compliant vehicles can automatically follow speed limits. However, non-compliant vehicles will attempt to pass the moving bottleneck created by the compliant vehicle. This project builds a multi-class cell transmission model to represent the relation between traffic flow parameters. This model can calculate flows of both compliant and non-compliant vehicles. An algorithm is proposed to calculate variable speed limits for each cell of the cell transmission model. This control algorithm is designed to reduce the stop-and-go behavior of vehicles at traffic signals. Simulation is used to test the effects of VSLs on an example network. The result shows that VSL is effective at reducing the energy consumption of the whole system and reduce the likelihood of crash occurrence.

17. Document Analysis/Descriptors	18. Availability Statement
Variable speed limits, Intersections, Connected vehicles, Autonomous vehicles, Bottlenecks, Traffic flow, Traffic safety, Algorithms	No restrictions. Document available from: National Technical Information Services, Alexandria, Virginia 22312

19. Security Class (this report)	20. Security Class (this page)	21. No. of Pages	22. Price
Unclassified	Unclassified	42	

Improving Intersection Safety Through Variable Speed Limits For Connected Vehicles

FINAL REPORT

prepared by:

Michael W. Levin
Rongsheng Chen
Department of Civil, Environmental, and Geo- Engineering
University of Minnesota

Chen-Fu Liao
Department of Mechanical Engineering
University of Minnesota

Tab Zhang
Department of Computer Science and Engineering
University of Minnesota

May 2019

Published by:

Roadway Safety Institute
Center for Transportation Studies
University of Minnesota
200 Transportation and Safety Building
511 Washington Ave. SE
Minneapolis, MN 55455

Acknowledgements

The funding for this project was provided by the United States Department of Transportation's Office of the Assistant Secretary for Research and Technology for the Roadway Safety Institute, the University Transportation Center for USDOT Region 5 under the Moving Ahead for Progress in the 21st Century Act (MAP-21) federal transportation bill passed in 2012.

Contents

List of Figures

List of Tables

Executive Summary

Background and Approach

Variable speed limit (VSL) is a widely used technology to harmonize the traffic flow on the road and improve traffic safety. VSL updates the road speed limit based on the real-time traffic condition. Traditional VSL requires variable message signs installed on overhead sign bridges or on the roadside so that drivers can see the suggested speed limit and adjust their driving speeds. Its effectiveness is restricted by drivers' compliance. With the technologies of connected/autonomous vehicles (CAVs), many limitations of VSL can be resolved. CAVs can be programmed to always follow VSL and the speed limit message can be transmitted through infrastructure-to-vehicle communication so that there is no need for variable message signs.

In this project, the research team considers a new type of VSL implemented on urban roads with mixed traffic of CAVs and human vehicles. CAVs receive speed limit messages from controllers at intersections and are set to follow speed limits. They create moving bottlenecks whose size is related to the number of CAVs. The human vehicles behind can overtake the moving bottleneck if there is enough space for them to do so. Otherwise, these vehicles have to follow the CAVs with a speed equal to the variable speed limit.

In this project, the research team completed the following tasks:

- Task 1: Develop model to capture the traffic flow dynamics with partial market penetration of CAV.
  The research team developed a traffic flow model based on the cell transmission model which was able to calculate the traffic state (flow, density, and speed) under the effects of moving bottleneck.
- Task 2: Develop VSL algorithm to smooth the traffic flow on urban roads with traffic signals.
  The research team proposed a VSL control algorithm that considered signal timings of adjacent intersections. With this VSL algorithm, vehicles are more likely to pass the intersection during the green light instead of waiting at the intersection during the red light.
- Task 3: Test VSL algorithm with simulations under different scenarios.
  The research team designed different scenarios with different values of CAV market penetrations, demands, and free-flow speeds. The test result was based on simulations using a test network consisted of five links with four signalized intersections.
- Task 4: Analyze safety and energy efficiency of VSL control.
  The research team used Simpson's model to transform vehicle specific power to engine fuel consumption to test the effects on energy consumption. The research team also applied shockwave occurrence as the indicator of the likelihood of a road crash to analyze the safety effects of VSL.

Key Findings

There are some findings regarding the efficiency and safety of VSL.

- The proposed VSL algorithm saves energy compared with a network without VSL control.
- The energy saving of VSL increases with market penetration and does not have strong relationships with demand and free-flow speed.
- The proposed VSL algorithm increases average vehicle travel time on long links.
- The proposed VSL algorithm reduces the deviance of shockwave occurrence when the CAV market penetration increases.

- The proposed VSL algorithm helps harmonize traffic condition by damping out shockwaves when CAV market penetration is large.

1 Introduction

Connected/autonomous vehicles (CAVs) offer many intelligent transportation system technologies to improve traffic safety and reduce the environmental impact. One such technology advanced the use of variable speed limits (VSLs). Numerous previous studies have investigated variable speed limits (VSL) for reducing traffic congestion and improving safety (Khondaker and Kattan, 2015). VSLs can also be used to reduce the environmental impact by reducing deceleration-acceleration cycles caused by intersection controls (Zhu and Ukkusuri, 2018). However, when used with legacy (human-driven) vehicles, VSL effectiveness is limited by the placement of VSL signs, driver limitations, and enforcement. VSL requires variable message signs, which are a significant infrastructure cost, limiting how frequently and on which roads speed limits may be changed. Human drivers also have limited precision in maintaining speed limits; speed limits are usually rounded to the nearest 5 mi/hr or km/hr, and human drivers may not effectively follow VSLs that change frequently in space or time. Finally, VSL effectiveness requires a high degree of driver compliance (Hellinga and Mandelzys, 2011). Kwon et al. (2007) found that compliance decreased as the difference between the VSL and the speed of approaching flow increased. Wasson et al. (2011) found that 75% of probe vehicles exceeded work zone (non-variable) posted speed limits during peak enforcement.

In contrast, CAVs could easily comply with VSLs. Vehicle-to-infrastructure communications and control technologies could be used to broadcast VSLs to connected vehicles, and autonomous driving could follow VSLs at a high degree of precision. CAVs could be directed to travel at speed limits with decimal values, and VSLs could be updated at small spatial-temporal intervals. Of course, it will be a long time before CAVs reach full market penetration. Therefore, our objective in this study is to study VSLs under partial CAV market penetration. We define two types of vehicles. Compliant vehicles (i.e. CAVs) follow VSLs, and non-compliant vehicles try to maintain the free flow speed whenever possible.

Compliant vehicles can, in some cases, enforce VSLs for non-compliant vehicles by forming a moving bottleneck. Therefore, a major component of this study is the development of a new flow model with moving bottlenecks formed through VSLs. The trapezoidal fundamental diagram was modified to represent the relation between traffic flow parameters. In Zhu and Ukkusuri (2018), cell transmission model (CTM) (Daganzo, 1994) was used to model the behavior of vehicles and exit flows of cells was modified to control the proactive driving behavior of connected vehicles. The effect of VSL on traveling speed and emissions was also discussed. In their model, the legacy vehicles were not allowed to pass the connected vehicles that follow the speed limit. Unlike Zhu and Ukkusuri (2018), this study builds a multi-class CTM that formulates the moving bottleneck generated by connected vehicles and the overtake behaviour of legacy (human-driven) vehicles.

As a potential effect of VSL, the sudden change of traffic flow can generate discontinuities in the traffic stream in the form of kinematic shockwaves. A shock wave is a rapid change in traffic conditions (flow and density) that propagates in time and space (van Driel, 2007). A forward moving shockwave propagates in the same direction as the traffic, while a backward moving shockwave propagates upstream of the disturbance. If drivers cannot react to the shockwave in time, a crash may happen. Therefore, it is important to analyze the safety effect of the VSL algorithm.

In this project, the research team used the CTM to model the traffic flow on arterial roads with traffic signals under the control of VSL. The CTM was modified to reflect the interaction between compliant vehicles that always follow the variable speed limit and non-compliant vehicles that may pass the moving bottleneck created by compliant vehicles. the research team proposed a VSL control algorithm that can reduce the probability of vehicles stopping at the intersection at the urban roads and save fuel consumption of vehicles. Then simulations were used to test the effectiveness of the VSL algorithm. Shockwave occurrence was used as an indicator to evaluate the likelihood of a crash occurrence under the control of VSL.

The structure of the remaining part of this report is as follows: Section 2 introduces the relevant literature about the VSL algorithm and traffic safety evaluation methods. Section 3 proposes a traffic flow model based on the CTM to represent the traffic flow dynamics under partial market penetration of connected and autonomous vehicles. Section 4 designs a VSL algorithm to reduce the energy consumption and improve the safety of vehicles on urban roads with signalized intersection. Section 5 analyzes the effects of energy consumption and the travel time of the proposed VSL algorithm by conducting sensitivity analysis varying the demand, free-flow speed, link length, and market penetration. Section 6 analyzes the safety effects of the proposed VSL algorithm.

2 Literature Review

This section is a collection of relevant literature about VSL control applied on freeways, urban roads, and the safety evaluation of VSL.

2.1 VSL algorithms on freeway

The VSL algorithms for freeways are designed to enhance the traffic safety and efficiency by modifying speed limits on different sections on a freeway. Hegyi et al. (2003, 2005b) constructed model predictive control (MPC) with macroscopic traffic flow model METANET and proposed a discretization method to calculate the optimal speed limits. They showed that VSL was effective in mitigating the shockwave and reducing total travel time. Hegyi et al. (2005a) compared the effect of VSL based on MPC models with traditional main-stream metering control. The study showed that the VSL was more effective than main-stream metering in preventing shockwaves. Abdel-Aty et al. (2006) used microscopic simulation to evaluate the safety effect of VSL and concluded that VSL was preferred during off-peak periods but was not recommended during peak periods. Hellinga and Mandelzys (2011) explored the effect of driver compliance to the implementation of VSL using microscopic traffic simulator PARAMICS and found that an increase in speed limit compliant could increase the benefit of VSL in safety. Talebpour et al. (2013) used a reactive speed selection algorithm integrated with a wavelet transformation based algorithm to apply VSL in a microscopic simulation model. Their VSL was shown to be effective in preventing the breakdown of the system. Hadiuzzaman and Qiu (2013) developed a modified CTM to test the effect of VSL on freeways. The result showed that VSL was most effective in saving travel time on congested road sections. On freeways, vehicles are never forced to stop by the traffic light so all these algorithms did not consider the effects of traffic signals and these VSL algorithms designed for freeways may not be effective on arterial roads.

2.2 VSL algorithms on urban roads

There are some studies focused on the speed planning strategy and the VSL control of vehicles at urban roads with signalized intersections, and these strategies help reduce fuel consumption or emission on urban roads by minimizing stop-and-go behaviours at traffic lights.

Sanchez et al. (2006) designed a driving model for individual drivers that considered upcoming signals. Simulation with a fleet of ten vehicles showed that the new model can reduce the energy consumption by 30%. Barth et al. (2011) proposed a dynamic speed planning algorithm to adjust vehicle speeds on an arterial road with known traffic signals. The velocity profiles for accelerating and decelerating vehicles were predefined using trigonometric functions. Using a simulation of a passenger sedan, the result showed that the algorithm reduced the fuel consumption by about 12%. Asadi and Vahidi (2011) used a MPC framework to calculate the optimal speed control of vehicles. The model was simulated using two fleets of vehicles with or without speed control equipment respectively. The model was shown to reduce the fuel consumption by 47% when applied to an arterial road with nine intersections in simulation. He et al. (2015) obtained the analytical solution of optimal vehicle trajectory of a multi-stage optimal control formulation considering vehicular queues and traffic signals. Ubiergo and Jin (2016) proposed a green driving strategy which saved fuel consumption by 8%. The model was simulated under different penetration rates of vehicles equipped with advisory speed limit systems. He et al. (2017) proposed a jam-absorption strategy based on Newell's car-following theory. Two simulation scenarios showed that this strategy was able to mitigate the traffic oscillations for a vehicle fleet. Zhu and Ukkusuri (2018) used cell transmission model (Daganzo, 1994) to model the traffic flow dynamics, In their model, links were divided into multiple homogeneous cells. To ensure vehicles arrive the intersection when the green light was on, connected vehicles that may arrive earlier at the intersection were locked in cells for several time steps and human vehicles were unable to pass autonomous vehicles in their model. The simulation result showed that the proposed control algorithm could reduce the emission by about 75% for a single link and by about 50% for Manhattan downtown network.

In aforementioned studies, some focused on the optimization of trajectories for an individual vehicle while ignoring the interaction between vehicles, some ignored the interaction between different types of vehicles with speed advisory systems. Interactions between equipped and unequipped vehicles can affect the implementation of VSL, so modelling intersections between these two types of vehicles makes results of simulations more realistic. With microscopic car-following models, vehicle interactions can be represented properly. However, compared with macroscopic or mesoscopic models, microscopic models take much more time to run and are relatively harder to calibrate. This problem is more pronounced when the simulation was conducted on a large network, such as a city-wide network. The study of Zhu and Ukkusuri (2018) considered the intersection between connected and unconnected vehicles, but it did not model vehicles passing a moving bottleneck.

2.3 VSL safety evaluation

In the literature, several crash risk evaluation models were developed using data from advanced traffic surveillance systems such as loop detectors and speed sensors. Crash models were developed by identifying and matching traffic conditions prior to crash occurrence using approaches such as logistic regression (Lee et al., 2006), neural network (Pande and Abdel-Aty, 2006), Bayesian logistic regression (Ahmed et al., 2012), and support vector machine (Yu and Abdel-Aty, 2013).

In addition, several Traffic Conflict Techniques (TCT) have been developed for traffic safety analysis, with their applications mainly limited to intersection conflicts. In TCT-based safety analysis, many objective measures have been developed and can be broadly classified into four groups: time-based, distance-based, deceleration-based and other composite measures (Yang et al., 2010).

Variable Speed Limit (VSL) has been applied in several European countries as a traffic operation and management technique for preventing accidents and improving traffic conditions (Cho and Kim, 2012). Various VSL strategies were developed by researchers as dynamic traffic control devices to improve traffic conditions and increase safety (Khondaker and Kattan, 2015). Many VSL systems have been implemented worldwide (Kress et al., 2018). Martinez and Jin (2018) investigated the optimal location for VSL application.

VSL systems (VSLs) have been modeled through microscopic simulation to study traffic flow changes and potential safety improvements (Abdel-Aty et al., 2006; Lee et al., 2006; Charly and Mathew, 2017). For example, Lee et al. (2006) developed a crash prediction model in a microsimulation to estimate crash potential for different control strategies of variable speed limits. The simulation results indicated that total crash potential over the entire freeway segment could be significantly reduced under variable speed limit control with a minimal increase in travel time compared to the fixed speed limit.

Surrogate safety models and measures were proposed in the literature to compute time to collision (TTC) between each pair of vehicles (Gousios et al., 2009; Hou et al., 2014; Charly and Mathew, 2017; Astarita et al., 2019). Probability of collision measures were used for safety analysis by comparing the computed TTC and a threshold TTC for scenarios with different VSL compliance rates (Bachmann et al., 2011; Khondaker and Kattan, 2015). Conran and Abbas (2018) developed a driver compliance model for VSL in a microscopic simulator. Downey (2015) and Nissan (2010) used the standard deviation of speeds to evaluate harmonization potential of VSL systems. Traffic flow variables such as headway and lane distribution were also used in "before-and-after" studies, or compared the test site with a control site to assess VSL systems' ability to harmonize and improve safety (Downey, 2015).

Abdel-Aty et al. (2006) and Lee et al. (2006) separately evaluated the impact of VSLs responses to real-time measures of Crash Potential (CP) in microscopic simulation models. The overall expected benefits of a VSLs application from their studies were unclear. Allaby et al. (2007) evaluated the safety impact of a VSLs control algorithm on a congested highway. They suggested that the implementation of VSLs could improve safety at a cost of increased travel times.

Chambers et al. (2017) found little change of lane speed differential and mixed results of crash reduction after the implementation of VSL on a corridor in Oregon. Mudgal and Hourdos (2017) analysed a section of a freeway corridor that the highest crash rate in the Twin Cities metropolitan area in MN. They observed traffic speed from video data and use the speed at the on-set of congestion as a surrogate measure to evaluate the rear-end collisions and near crashes after and before the implementation of a VSL strategy. They found the previous VSL strategy did not significantly improve the crash rate at the congested area with 2 successive bottlenecks. Qu et al. (2017) conducted a statistical analysis using empirical traffic data from a European motorway with VSL control strategy. They found that VSL can effectively reduce the mean speed and the percentage of small space headways. However, the qualitative analysis implied that continuously reducing the speed limit below a certain threshold would not lead to better safety benefits.

Breton et al. (2002) used a model predictive control (MPC) approach to optimally coordinate variable speed limits for highway traffic. They found that dynamic speed limits can create traffic conditions to faster damp out shockwaves. Lee and Volpatti (2010) examined how shockwaves affect the likelihood of crash occurrence on freeways. Their results showed that crashes are more likely to occur when the forward shockwave speed is lower. This indicated that slower vehicle progression in near-capacity conditions and slower dissipation of a queue in congested conditions are more likely to cause crashes.

Connected and Autonomous Vehicles (CAVs) incorporate many intelligent transportation technologies, i.e., VSLs, to improve traffic flow and safety. Qi et al. (2019) evaluated the impact of a Connected Vehicles (CVs) based VSL field test on I-5 corridor in Seattle, WA. The results indicated that CVs alleviate the congestion and decrease the speed of congestion expanding and the speed deviation is significantly influenced by traffic condition, driver compliance, and road characteristics.

The safety analysis of our study focused on the assessment of VSL strategy in a traffic network with various numbers of CVs. The research team studied VSL systems by including two types of vehicles (i.e., compliant and non-compliant vehicles) under partial CAV market penetration in a mesoscopic simulation model. The compliant vehicles (i.e. CAVs) follow VSLs, and the non-compliant vehicles try to maintain the free flow speed whenever possible. A modified multi-class cell transmission model (CTM) was developed to model the traffic flow for both Connected Vehicles (CV) and legacy vehicles (i.e., human drivers).

3 Traffic Flow Model

In this project, the effects of VSL on energy consumption and safety are both derived from the effect of VSL on the traffic flow. So we first need to build a traffic flow model that can capture the effect of VSL on the speed, density, and flow of the road network.

We classify vehicles as either *compliant* or *non-compliant*. Compliant vehicles are expected to be connected automated vehicles that receive and obey VSL instructions at high spatial-temporal resolutions. Non-compliant vehicles are typically non-automated (legacy) vehicles. Compliant vehicles may force vehicles behind them to slow down as well by creating a *moving bottleneck*, thus allowing a small market penetration of compliant vehicles to have a disproportionate effect on the link speed.

Let $\mathscr{G} = (\mathscr{N}, \mathscr{A})$ be a traffic network with nodes $\mathscr{N}$ and links $\mathscr{A}$. Consider a single link in $\mathscr{A}$. This section seeks to model the evolution of density and flow within the link, accounting for moving bottlenecks. We develop a general model of traffic flow, and discuss how to choose VSLs in Section 4. Our objective is to obtain a cell transmission model that can be used for the dynamic simulation of flows along a link, taking the VSLs per cell-time as parameters to the simulation. We first define the effects of moving bottlenecks on the trapezoidal flow-density relationship before extending the model to multiclass flows and developing the Godunov (1959) approximation.

3.1 Moving bottleneck flow-density relationship

Let $k(t,x)$ and $q(t,x)$ be the density and flow at spatial point x and time t, respectively. Let $s(t,x)$ be the VSL at (t,x), with the caveat that only compliant vehicles obey $s(t,x)$. Non-compliant vehicle speeds are determined by the standard speed-density relationship. As with previous work on the cell transmission model (Daganzo, 1994, 1995), we assume a trapezoidal fundamental diagram:

$$f(k(t,x)) = \min\{vk(t,x), Q, w(K - k(t,x))\} \tag{1}$$

where v is the free flow speed, w is the congested wave speed and is a negative number, Q is the capacity, and K is the jam density.

When $s(t,x) < v$, compliant vehicles may form a moving bottleneck travelling at speed $s(t,x)$. The VSL $s(t,x) \leq v$ is the maximum speed of the moving bottleneck, but compliant vehicles may still travel at a speed slower than $s(t,x)$ if traffic is sufficiently congested. The moving bottleneck has a modified fundamental diagram:

$$f^{\mathrm{b}}(k(t,x)) = \min\{s(t,x)k(t,x), Q, w(K - k(t,x))\} \tag{2}$$

Let $\delta(t,x)$ be the number of lanes blocked by moving bottlenecks at (t,x). Let ℓ be the number of lanes; then $\delta(t,x) \in [0,l]$. If $s(t,x) < v$, and $\delta(t,x) > 0$, then the moving bottleneck will cause one of three situations (Daganzo and Laval, 2005; Simoni and Claudel, 2017):

1. Traffic is at free flow, but enough capacity remains that regular traffic can overtake the moving bottleneck.

2. The moving bottleneck is active, and there is not enough capacity for regular traffic to overtake it. Some non-compliant vehicles are obstructed by the bottleneck.

3. The moving bottleneck is inactive because the speed of the traffic is lower than the VSL.

We define two types of flow at (t,x): the *passing flow* $q^{\mathrm{p}}(t,x)$ is the flow passing the moving bottleneck, and the *bottleneck flow* $q^{\mathrm{b}}(t,x)$ is the flow from vehicles travelling with or behind the bottleneck. We first discuss each case separately to develop the combined flow-density relationship.

Case 1

Case 1 occurs when all flow can pass the moving bottleneck. Since the moving bottleneck obstructs $\delta(t,x)$ lanes, then $l-\delta(t,x)$ lanes are available for passing. If vehicles pass the moving bottleneck at speed $u(t,x)$, then the passing flow is

$$q^{\mathrm{p}}(t,x) = \min\left\{vk(x,t), Q\left(\frac{\ell-\delta(t,x)}{\ell}\right)\right\} \tag{3}$$

Although congested flow with speed $u(t,x) > s(t,x)$ may still be able to overtake a moving bottleneck, if $u(t,x) < v$ then the flow is limited by Q or $w(K-k(t,x))$ from equation (1), and will therefore be partially restricted by the moving bottleneck (case 2). Therefore, in case 1, passing flow must travel at speed v. Since all flow overtakes the bottleneck in case 1, $q^{\mathrm{b}}(t,x)$ consists solely of bottleneck vehicles.

Case 2

In case 2, the moving bottleneck obstructs $\delta(t,x)$ lanes. Flow on the remaining $l-\delta(t,x)$ lanes is determined by equation (1):

$$q^{\mathrm{p}}(t,x) = \left(\frac{\ell-\delta(t,x)}{\ell}\right)\min\{Q, w(K-k(t,x))\} \tag{4}$$

The uncongested constraint $q^{\mathrm{p}}(t,x) \leq vk(t,x)$ is not relevant to case 2; if the uncongested constraint were active, case 1 would hold instead. The flow in the remaining lanes, $q^{\mathrm{b}}(t,x)$, is determined by the moving bottleneck flow-density relationship (2):

$$q^{\mathrm{b}}(t,x) = \min\left\{s(t,x)k(t,x), \left(\frac{\delta(t,x)}{\ell}\right)Q, \left(\frac{\delta(t,x)}{\ell}\right)w(K-k(t,x))\right\} \tag{5}$$

Case 3

Case 3 occurs when

$$s(t,x) > u(t,x) = \frac{\min\{Q, w(K-k(t,x))\}}{k(t,x)} \tag{6}$$

which results in all vehicles, including the bottleneck vehicle, moving at $u(t,x)$. Flow may remain at capacity although the speed will be less than free flow speed. The passing and bottleneck flows are therefore determined by equation (1):

$$q^{\mathrm{p}}(t,x) = \frac{\ell-\delta(t,x)}{\ell}\min\{Q, w(K-k(t,x))\} \tag{7}$$

$$q^{\mathrm{b}}(t,x) = \frac{\delta(t,x)}{\ell}\min\{Q, w(K-k(t,x))\} \tag{8}$$

The above three cases can be combined into a single flow-density relationship that depends on $s(t,x)$ and $\delta(t,x)$. The passing flow follows equation (1):

$$q^{\mathrm{p}}(t,x) = \min\left\{vk(t,x), \left(\frac{\ell-\delta(t,x)}{\ell}\right)Q, \left(\frac{\ell-\delta(t,x)}{\ell}\right)w(K-k(t,x))\right\} \tag{9}$$

The bottleneck flow is

$$q^{\mathrm{b}}(t,x) = \min\left\{ s(t,x)k(t,x) - q^{\mathrm{p}}(t,x), \left(\frac{\delta(t,x)}{\ell}\right)Q, \left(\frac{\delta(t,x)}{l}\right)w(K-k(t,x)) \right\} \tag{10}$$

when passing flow constraints $q^{\mathrm{p}}(t,x) \leq \left(\frac{\delta(t,x)}{\ell}\right)Q$ or $q^{\mathrm{p}}(t,x) \leq \left(\frac{\delta(t,x)}{\ell}\right)w(K-k(t,x))$ are active. Otherwise, the bottleneck flow consists solely of the moving bottleneck vehicle(s). The uncongested regime term $s(t,x)k(t,x) - q^{\mathrm{p}}(t,x)$ is the flow that is unable to pass the bottleneck.

3.2 Multiclass flow

Section 3.1 defines the flow-density relationship for a moving bottleneck blocking $\delta(t,x)$ lanes. To determine $\delta(t,x)$, we must track multiple classes of flow—compliant and non-compliant vehicles. In addition, the flow model of Section 3.1 is primarily useful for a low market penetration of compliant vehicles. If compliant vehicles make up a significant fraction of the density, moving bottlenecks may be comprised of platoons of (as opposed to individual) compliant vehicles, and the bottleneck flow $q^{\mathrm{b}}(t,x)$ must be revised accordingly. We now add a class index to flows and densities.

In Section 3.1, the moving bottleneck was a moving point in space that limited the speed of vehicles behind it. When considering compliant vehicle platoons, the moving bottleneck may no longer be reduced to a single point in space, but may consist of a platoon. We therefore define a *moving bottleneck* as the front bumper of any compliant vehicle or platoon of compliant vehicles. A platoon of compliant vehicles is a single-lane group of compliant vehicles that excludes non-compliant vehicles. Non-compliant vehicles that merge into the middle of a compliant platoon break up the compliant platoon into two smaller platoons, each with a separate moving bottleneck.

Let $k^m(t,x)$ and $q^m(t,x)$ be the density and flow of class m at (t,x), respectively. We consider two classes: compliant ($m=\mathrm{c}$) and non-compliant ($m=\mathrm{n}$). Note that $q^m(t,x)$ cannot be proportionally split among passing and bottleneck flows because compliant vehicles are always included in bottleneck flow. The number of lanes obstructed by the moving bottleneck, $\delta(t,x)$, also depends on the class-proportions of densities.

Equation (9) must be revised to account for limited market penetrations of non-compliant vehicles:

$$q^{\mathrm{n,p}}(t,x) = \min\left\{ \begin{array}{l} vk^{\mathrm{n}}(t,x), \\ \left(\frac{\ell-\delta(t,x)}{\ell}\right)Q, \\ \left(\frac{\ell-\delta(t,x)}{\ell}\right)w(K-k^{\mathrm{c}}(t,x)-k^{\mathrm{n}}(t,x)) \end{array} \right\} \tag{11}$$

where $q^{m,\mathrm{p}}(t,x)$ is the passing flow of class m. By definition $q^{\mathrm{c,p}}(t,x)=0$ (all compliant vehicles follow the moving bottleneck speed). If $q^{\mathrm{n,p}}(t,x) = vk^{\mathrm{n}}(t,x)$, then all non-compliant vehicles are able to pass in the unblocked $l-\delta(t,x)$ lanes. Otherwise, flow is restricted by the congested regime constraints which apply to all vehicles.

Similarly, equation (10) must be revised because all compliant vehicles will become part of the moving bottleneck flow. Non-compliant vehicles may also be included in the bottleneck flow if they are stuck behind a moving bottleneck. The total bottleneck flow is

$$q^{\mathrm{n,b}}(t,x) + q^{\mathrm{c,b}}(t,x) = \min\left\{ \begin{array}{l} s(t,x)\left(k^{\mathrm{n}}(t,x)+k^{\mathrm{c}}(t,x)\right) - q^{\mathrm{n,p}}(t,x), \\ \left(\frac{\delta(t,x)}{\ell}\right)Q, \\ \left(\frac{\delta(t,x)}{\ell}\right)w(K-k^{\mathrm{c}}(t,x)-k^{\mathrm{n}}(t,x)) \end{array} \right\} \tag{12}$$

where $q^{m,\mathrm{b}}(t,x)$ is the bottleneck flow of class m. Note that equations (11) and (12) do not depend on the proportion of density in the passing and bottleneck lanes. The total density may be asymmetrically distributed among passing and bottleneck lanes because non-compliant vehicles will prefer to pass whenever possible. However, if the density is high enough, the capacity of the passing lanes will be insufficient for all non-compliant vehicles, and some will be forced to remain in the bottleneck lane. The number of bottleneck lanes at any point (t,x) is equal to

$$\frac{\delta(t,x)}{\ell} = \frac{k^{\mathrm{c}}(t,x)}{k^{\mathrm{n}}(t,x)+k^{\mathrm{c}}(t,x)} \tag{13}$$

Although $\delta(t,x)$ is actually the *number* of lanes blocked, we extend it to real number values to match the kinematic wave theory. At small spatial or temporal intervals, equation (13) might be determined by fractions of vehicles.

When using equation (13) for the number of bottleneck lanes, (12) is entirely comprised of compliant vehicles. From equation (12), the desired flow through the bottleneck lanes is

$$s(t,x)\left(k^{\mathrm{n}}(t,x)+k^{\mathrm{c}}(t,x)\right)-q^{\mathrm{n,p}}(t,x)$$

and the density of vehicles in the bottleneck lanes is thus

$$\left(k^{\mathrm{n}}(t,x)+k^{\mathrm{c}}(t,x)\right)-\frac{q^{\mathrm{n,p}}(t,x)}{u^{\mathrm{n,p}}(t,x)}$$

The compliant-vehicle portion of that density is

$$\frac{k^{\mathrm{c}}(t,x)}{\left(k^{\mathrm{n}}(t,x)+k^{\mathrm{c}}(t,x)\right)-\frac{q^{\mathrm{n,p}}(t,x)}{u^{\mathrm{n,p}}(t,x)}}$$

which gives an equation for the compliant portion of the bottleneck flow:

$$q^{\mathrm{c,b}}(t,x) = \frac{k^{\mathrm{c}}(t,x)}{\left(k^{\mathrm{n}}(t,x)+k^{\mathrm{c}}(t,x)\right)-\frac{q^{\mathrm{n,p}}(t,x)}{u^{\mathrm{n,p}}(t,x)}}\left(q^{\mathrm{n,b}}(t,x)+q^{\mathrm{c,b}}(t,x)\right) \tag{14}$$

Since $q^{\mathrm{c,b}}(t,x) = u^{\mathrm{c,b}}(t,x)k^{\mathrm{c,b}}(t,x)$, equation (14) can be simplified to

$$q^{\mathrm{c,b}}(t,x) = \left(q^{\mathrm{n,b}}(t,x)+q^{\mathrm{c,b}}(t,x)\right) \tag{15}$$

with $q^{\mathrm{n,b}}(t,x)=0$. which indicates, unsurprisingly, that all flow in the bottleneck lanes is due to compliant vehicles when the bottleneck lanes are determined by the proportion of compliant vehicles in the density. Based on equations (14) and (15), equation (12) can be rewritten as

$$q^{\mathrm{c,b}}(t,x) = \min\left\{\begin{array}{l} s(t,x)k^{\mathrm{c}}(t,x), \\ \left(\frac{\delta(t,x)}{\ell}\right)Q, \\ \left(\frac{\delta(t,x)}{\ell}\right)w\left(K-k^{\mathrm{c}}(t,x)-k^{\mathrm{n}}(t,x)\right) \end{array}\right\} \tag{16}$$

because if constraint

$$q^{\mathrm{c,b}}(t,x) \leq s(t,x)\left(k^{\mathrm{n}}(t,x)+k^{\mathrm{c}}(t,x)\right)-q^{\mathrm{n,p}}(t,x) \tag{17}$$

is active, then $q^{\mathrm{n,p}}(t,x) = s(t,x)k^{\mathrm{n}}(t,x)$ from the passing lanes.

It is important to clarify the behavioral implications. At point (t,x), the non-compliant vehicles may move forward at a faster rate than the compliant vehicles. Thus, the compliant vehicles will tend to accumulate at certain trajectories in space-time, increasing the proportion of compliant-vehicle density along those trajectories. Eventually, non-compliant vehicles will become less able to pass the compliant-vehicle trajectories, which will result in the compliant vehicles fulfilling their role as a moving bottleneck. Therefore, it is necessary to consider the behaviour over a larger space-time horizon, rather than individual points, when analysing the effect of compliant vehicles on overall speeds.

3.3 Cell transmission model

The cell transmission model developed here uses the three-case bottleneck logic of Simoni and Claudel (2017) and chooses $\delta(t,x)$ by equation (13). As in the standard kinematic wave theory (Lighthill and Whitham, 1955; Richards, 1956), flows and densities of all classes must satisfy the conservation law

$$\frac{\partial q^m(t,x)}{\partial x} = -\frac{\partial k^m(t,x)}{\partial t} \tag{18}$$

Combining equation (18) with the flow-density relationship equations (11) and (16) results in a system of partial differential equations. Since this kinematic wave theory is difficult to solve exactly, we develop a cell transmission model to approximate it.

Recall that this model is concerned with flow on a single link. Divide the link into *cells* of length Δx, and divide time into *time steps* of length Δt such that

$$v = \frac{\Delta x}{\Delta t} \tag{19}$$

to satisfy the Courant et al. (1967) condition. We assume that density is evenly distributed throughout each cell, and that the VSL is uniform per cell. Let $n_i^m(t)$ be the occupancy of class m of cell i at time step t, and let $y_{ij}^m(t)$ be the flow from cell i to cell j at time step t. Let $\delta_i(t)$ be the number of lanes blocked by moving bottlenecks, and let $s_i(t)$ be the speed of the compliant vehicles, in cell i at time step t. Let $N = K\Delta x$ be the maximum cell occupancy. Cell occupancy evolves as follows:

$$n_j^m(t+1) = n_j^m(t) + y_{ij}^m(t) - y_{jk}^m(t) \tag{20}$$

Transition flows are split for compliant and non-compliant vehicles, and are calculated similar to equations (11) and (12). The flow passing the bottleneck, $y_{ij}^{\mathrm{p},m}(t)$, is

$$y_{ij}^{\mathrm{n,p}}(t) = \min\left\{ n_i^{\mathrm{n}}(t), \frac{\ell - \delta_i(t)}{\ell} Q\Delta t, \frac{\ell - \delta_i(t)}{\ell} \frac{w}{v} \left(N - n_j^{\mathrm{c}}(t) - n_j^{\mathrm{n}}(t)\right) \right\} \tag{21}$$

with $y_{ij}^{\mathrm{p,c}}(t) = 0$. As in equation (12), the flow moving with the bottleneck is

$$y_{ij}^{\mathrm{c,b}}(t) = \min \left\{ \begin{array}{l} \frac{s_i(t)}{v} n_i^{\mathrm{c}}(t) \\ \left(\frac{\delta_i(t)}{\ell}\right) Q\Delta t, \\ \left(\frac{\delta_i(t)}{\ell}\right) \frac{w}{v}(N - n_j^{\mathrm{c}}(t) - n_j^{\mathrm{n}}(t)) \end{array} \right\} \tag{22}$$

with

$$\frac{\delta_i(t)}{\ell} = \frac{n_i^{\mathrm{c}}(t)}{n_i^{\mathrm{n}}(t) + n_i^{\mathrm{c}}(t)} \tag{23}$$

The v denominator in equations (21) and (22) arises from dividing by $\frac{\Delta x}{\Delta t}$ to convert $k^m(t,x)$ and $q^m(t,x)$ into $n_i^m(t)$ and $y_{ij}^m(t)$, and Δx is chosen so that $\frac{\Delta x}{\Delta t} = v$ to satisfy the Courant et al. (1967) condition.

When $s_i(t) < v$, equation (22) requires that not all bottleneck flow exit the cell. This behaviour follows from the choosing the cell length such that vehicles travel one cell per time step at the free flow speed. Therefore, at slower speeds, including those caused by VSLs, some vehicles must remain in the cell even in uncongested conditions.

Proposition 1. *The cell transmission model* (20)–(23) *is a Godunov (1959) approximation to the moving bottleneck kinematic wave theory.*

Proof. Because $\frac{n_i^m(t)}{\Delta x} \approx k^m(t,x)$ and $\frac{y_{ij}^m(t)}{\Delta t} \approx q^m(t,x)$, equations (20), (21), and (22) are approximately equivalent to equations (18), (11), and (16), respectively. Equation (23) follows from equation (13). As in Daganzo (1994), this results in a discrete space-time approximation of the kinematic wave theory. □

4 VSL Control Algorithm

Having developed the flow model, we now move to choosing VSLs. Compliant vehicles provide a method for disproportionate enforcement of VSLs by forming a moving bottleneck. However, VSLs affect the positioning of compliant vehicles. For instance, in case 1 in Section 3.1, choosing a VSL less than free flow speed will not affect non-compliant flow, but the slower speed of compliant vehicles will relegate them to the back of the queue. Those compliant vehicles would be less able to create a moving bottleneck to enforce VSLs at later times. Therefore, the optimal choice of VSLs when non-compliant vehicles are present must take future traffic conditions into consideration.

Ideally, we would find the optimal VSL for each cell at each time step (For example, 6 seconds). This problem can be formulated as a mathematical program using the method of Ziliaskopoulos (2000). However, some of the constraints in equations (20)–(23) are quadratic, and the associated quadratic constraint matrix is not positive semi-definite. Therefore the mathematical program is not convex and is difficult to solve. Finding a global optimum of a non-convex problem is NP-hard. Instead, a heuristic VSL algorithm is proposed to control speed limits on a road segment to reduce the total energy consumption. In this algorithm, the speed limit of each road segment is calculated by an intelligent controller at the intersection. All compliant vehicles in the same road segment follow the same speed limit, and all non-compliant vehicles have speeds that are always smaller than the free flow speed of the link. To reduce energy consumption, vehicles need to reduce the severity of stop-and-go cycles. At signalized intersections, vehicles often come to a complete stop from a high travel speed and then wait for the next green light interval. After traffic light turns green, vehicles accelerate again to the speed limit or the target speed, which takes a lot of energy.

This VSL algorithm aims at reducing the acceleration of vehicles by forcing vehicles to reduce speeds so that they can pass the intersection during green light intervals. Figure 1 shows trajectories for two vehicles following different speed control strategies. Neither of them can reach the intersection with the remaining green light time. V_1 uses a higher speed to reach the intersection but catches a red light, while V_2 uses a lower speed and catches the next green light. After passing the signal, both vehicles accelerate to the free flow speed. V_1 requires greater acceleration because it came to a complete stop, and that acceleration uses more energy.

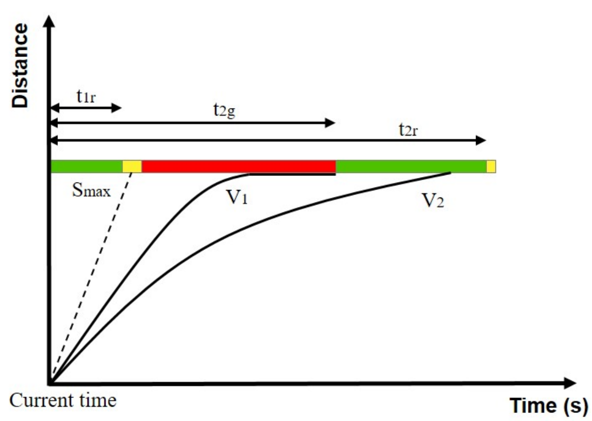

Figure. 1: The effect of variable speed limit on arterial roads

Assume intelligent controllers located at road intersections calculate speed limits for all vehicles on upcoming links and send calculated speed limits to these autonomous vehicles in every time step. When autonomous vehicles receive the information about speed limits, they will start to follow it. To calculate the speed limit, the time to the beginning of the ith green interval t_{ig} and the time to the end of the ith green interval t_{ir} were calculated first. If the light is currently green, then the 1_{st} green interval is the current green interval, and t_{1g} is set to be 0. Otherwise, the 1_{st} green interval is the following green interval. In Figure 1, green light is on at the moment, so t_{1g} is 0 and t_{1r} is the time from current time to the end of the green interval. t_{2g} and t_{2r} are the times from the current time to the beginning and the end of next green interval. The available time that a vehicle can use to pass through the intersection when the light is green can be represented by $[t_{1g}, t_{1r}] \cup [t_{2g}, t_{2r}]$. In this study, only the 1_{st} and the 2_{nd} green light intervals are considered to set the speed limit.

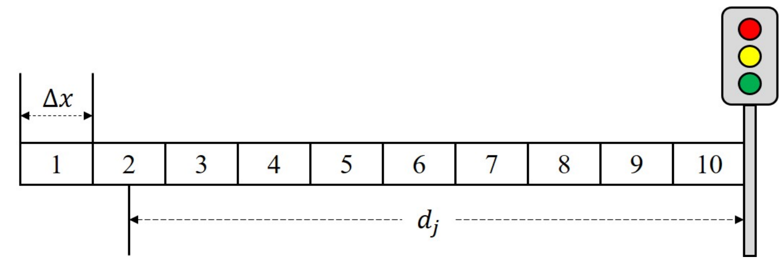

Figure. 2: Distance to the intersection

Figure 2 shows a link modelled by CTM. The link is divided into ten cells with the same size Δx. The distance from cell j to the intersection can be calculated using $d_j = (n - j + 0.5) * \Delta x$. n is the total cell number for a link. With times and distances, feasible ranges of travel speeds can be calculated. For cell j, corresponding speeds for t_{ig} and t_{ir} can be denoted by $v_{ig,j} = \frac{d_j}{t_{ig}}$ and $v_{ir,j} = \frac{d_j}{t_{ir}}$. If d_{1g} is 0, then its corresponding speed is set to be the maximum speed $S_{\max}$. There is another constraint for travel speeds which is defined by the maximum speed $S_{\max}$ and the minimum speed $S_{\min}$ as: $[S_{\min}, S_{\max}]$. The calculated variable speed limit should always lie between the maximum speed and the minimum speed. $S_{\min}$ is set to be 0 mile/h. The set $[v_{\text{low}}, v_{\text{up}}] = [v_{1g,j}, v_{1r,j}] \cap [S_{\min}, S_{\max}]$ is first calculated to be the feasible range for speed. If this set is empty, another set $[v_{2g,j}, v_{2r,j}] \cap [S_{\min}, S_{\max}]$ is used to be the feasible range for speeds. This means if a vehicle can pass through the intersection using the first green interval, it should use this interval instead of unnecessarily reducing its speed to wait for the second green interval. The speed limit of cell j is set to be the most energy-efficient speed in the feasible range under the same acceleration, which is $S_j = \underset{v \in [v_{low}, v_{up}]}{\arg\min} (P(v))$, where $P(v)$ is the energy consumption to travel a distance of Δx at speed v. If both time intersections are empty, it means vehicles in cell j have no chance to pass the intersection when the traffic light is green. If so, vehicles have no choice but to decelerate to a stop. The VSL of cell j is calculated with $S_j = \sqrt{2 d_j a}$. a is the deceleration rate. This formula ensures vehicles can stop at the intersection using the given deceleration distance. As d_j gets larger, S_j also gets larger. The value of a should guarantee that the value of S_j for any cell is smaller than the free flow speed. In this study, a is set to 0.22 mile/s^2.

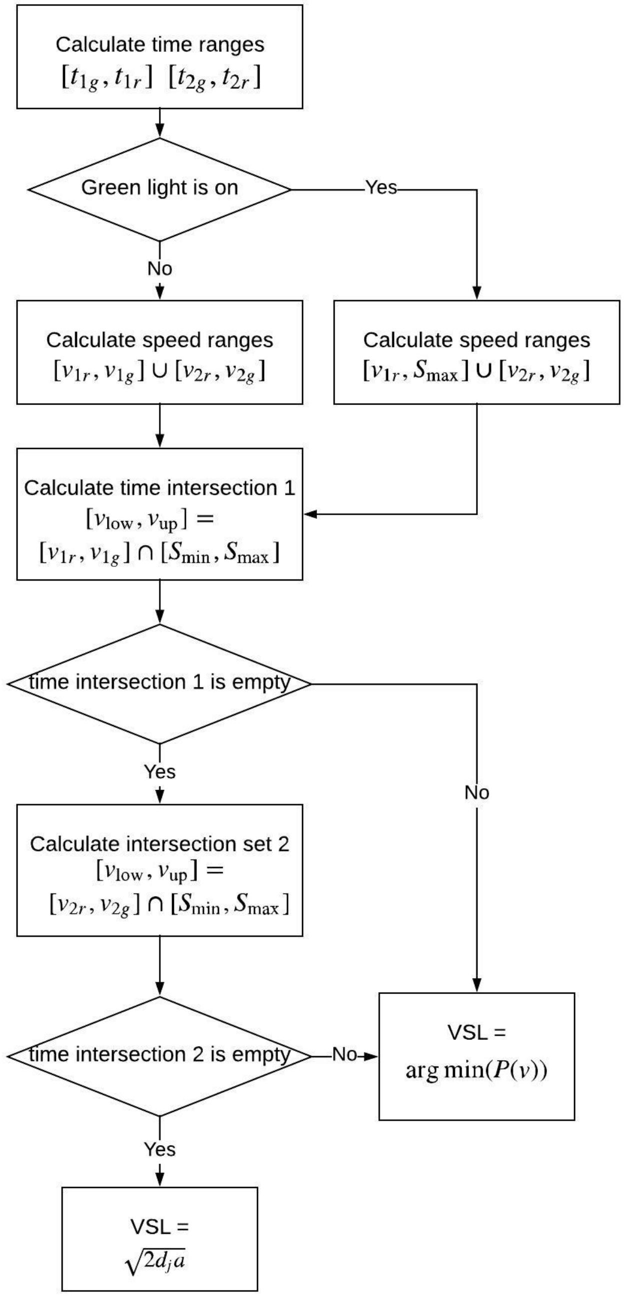

Figure. 3: VSL algorithm

Figure 3 shows the flowchart of the VSL algorithm. In this algorithm, only times to the beginning and the end of next green interval and the second green interval are considered, vehicles are assumed not to wait for the third and the fourth green intervals. This algorithm runs every time step to calculate the speed limit for every cell. The time to green t_{ig} and the time to red t_{ir} are updated every time step, as are the ranges of feasible speeds and speed limits.

5 Energy Consumption Analysis

A major motivation for VSLs is the smoothing of speed variations resulting in fewer acceleration-deceleration cycles. We apply the vehicle specific power-based energy consumption model of Levin et al. (2014) to the proposed traffic flow model to get the energy consumption.

5.1 Energy consumption model

5.1.1 Speed and acceleration

Since $y \approx q\Delta t$ and $n \approx k\Delta x$, the relationship $q = uk$ becomes

$$y^k_{ij}(t) = \frac{u^k_{ij}(t)}{v} n^k_i(t) \tag{24}$$

where $u^k_{ij}(t)$ is the speed of flow of type $k \in \{\mathrm{p},\mathrm{b}\}$ moving from i to j at time t. Equation (24) requires modification for passing and bottleneck flows, which may move at different speeds:

$$u^{\mathrm{p}}_{ij}(t) = v\frac{y^{\mathrm{p}}_{ij}}{\frac{\ell_i - \delta_i(t)}{\ell_i}\left(n^{\mathrm{n}}_i(t) + n^{\mathrm{c}}_i(t)\right)} \tag{25}$$

$$u^{\mathrm{b}}_{ij}(t) = v\frac{y^{\mathrm{b}}_{ij}}{\frac{\delta_i(t)}{\ell_i}\left(n^{\mathrm{n}}_i(t) + n^{\mathrm{c}}_i(t)\right)} \tag{26}$$

where $\frac{\delta_i(t)}{\ell_i}\left(n^{\mathrm{n}}_i(t) + n^{\mathrm{c}}_i(t)\right)$ is the number of vehicles behind a moving bottleneck. $u^{\mathrm{p}}_{ij} \le v$ and $u^{\mathrm{b}}_{ij}(t) \le v$ because of equations (20)–(23).

The kinematic wave theory is a first-order model and does not necessarily predict realistic acceleration values. Nevertheless, acceleration can still be estimated as the average rate of change in speed across time steps. We estimate the acceleration $a_{ij}(t)$ for bottleneck and passing flow separately:

$$a^{\mathrm{p}}_{ij}(t) = \frac{u^{\mathrm{p}}_{ij}(t) - u^{\mathrm{p}}_{ij}(t-1)}{\Delta t} \tag{27}$$

$$a^{\mathrm{b}}_{ij}(t) = \frac{u^{\mathrm{b}}_{ij}(t) - u^{\mathrm{b}}_{ij}(t-1)}{\Delta t} \tag{28}$$

The bottleneck flow speed $u^{\mathrm{b}}_{ij}(t)$ and acceleration $a^{\mathrm{b}}_{ij}(t)$ apply to the $\frac{\ell_i - \delta_i(t)}{\ell_i}\left(n^{\mathrm{n}}_i(t) + n^{\mathrm{c}}_i(t)\right)$ vehicles in the bottleneck lanes. Similarly, the $\frac{\delta_i(t)}{\ell_i}\left(n^{\mathrm{n}}_i(t) + n^{\mathrm{c}}_i(t)\right)$ vehicles in the passing lane have speed $u^{\mathrm{p}}_{ij}(t)$ and acceleration $a^{\mathrm{p}}_{ij}(t)$.

5.1.2 Vehicle specific power

Using speed and acceleration, we estimate vehicle specific power and energy consumption. Vehicle specific power was transformed into engine fuel consumption using an engine efficiency model based on Simpson (2005) with energy equivalence of 36.44kW·hr per gallon of fuel. Passenger sedan vehicle characteristics were also taken from Simpson (2005). All calculations are repeated for passing and bottleneck flows. We first calculate power applied to the wheels, $P_{ij}^{k,\text{wheel}}(t)$, as

$$P_{ij}^{k,\text{wheel}}(t) = \frac{1}{2}\rho C_{\text{D}} A u_{ij}^{k}(t)^3 + C_{\text{RR}} m g u_{ij}^{k}(t) + C_{\text{m}} m a_{ij}^{k}(t) u_{ij}^{k}(t) \tag{29}$$

where C_{D} and C_{RR} are the coefficients of friction for air resistance and rolling resistance, respectively, g is acceleration due to gravity, ρ is the density of air, A is the frontal area, C_{m} is the rotational inertia, and m is the vehicle mass. $\frac{1}{2}\rho C + \text{D} A u_{ij}^{k}(t)^3$ is the aerodynamic resistance, $C_{\text{RR}} m g u_{ij}^{k}(t)$ is the rolling resistance, and $C_{\text{m}} m a_{ij}^{k}(t) u_{ij}^{k}(t)$ is the power required for acceleration.

Some power is lost to inefficiencies in the drive train:

$$P_{ij}^{k,\text{drive\_loss}}(t) = \frac{1-\eta_{\text{trans}}}{\eta_{\text{trans}}} \left(P_{ij}^{k,\text{wheel}}(t) + C_{\text{m}} m a_{ij}^{k}(t) u_{ij}^{k}(t) \right) \tag{30}$$

where η_{trans} is the transmission efficiency. The engine power required, $P_{ij}^{\text{eng}}(t)$, is

$$P_{ij}^{k,\text{eng}}(t) = P_{ij}^{k,\text{wheel}}(t) + P_{ij}^{k,\text{drive\_loss}}(t) + P^{\text{acc}} \tag{31}$$

where P^{acc} is the power required for accessories such as the radio or air conditioning. Power lost to engine inefficiency is calculated as

$$P_{ij}^{k,\text{eng\_loss}}(t) = \frac{1-\eta_{\text{eng}}}{\eta_{\text{eng}}} P_{ij}^{k,\text{eng}}(t) \tag{32}$$

and the power in terms of fuel consumption, $P_{ij}^{k,\text{fuel}}(t)$, is

$$P_{ij}^{k,\text{fuel}}(t) = P_{ij}^{k,\text{eng}}(t) + P_{ij}^{k,\text{eng\_loss}}(t) \tag{33}$$

The energy consumption for moving from cell i to cell j for movement of type $k \in \{\text{p},\text{b}\}$ at time t is $P_{ij}^{k,\text{fuel}}(t)\Delta t$, and the number of vehicles moving from i to j is given by the cell transition flows.

5.2 Test network

A simple arterial network with 4 signalized intersections as illustrated in Figure 4 was used for energy consumption analysis. A simple 2-phase signal timing plan (as shown in Figure 5) with different offsets was implemented in the simulation model. Link 12 and 67 are centroid connectors used to send vehicles to the transportation network and remove vehicles from the network. Link 23, 34, 45, and 56 were modelled with the modified CTM. In CTM, the cell size of each cell is determined by the distance travelled at the free-flow speed during one time step (i.e., cell size = 6 sec x 30 mph = 0.05 miles for free-flow speed at 30 mph).

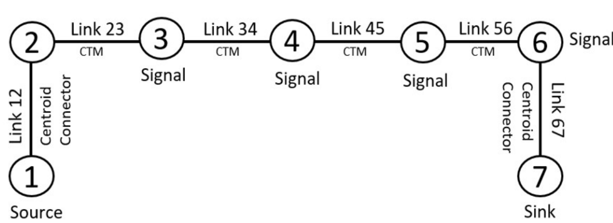

Figure. 4: Structure of the network in Table 1.

Figure. 5: Signal timing in Figure 4.

5.3 Energy consumption analysis results

This section presents simulation results obtained with the modified cell transmission model developed in section 3 for the efficiency of the VSL algorithm in various traffic conditions. We use a trapezoidal fundamental diagram. The jam density is 264 veh per mile, the time step is 6 seconds, and the demand input duration is 60 minutes. The energy consumption model used in this project was based on the sedan in the PAMVEC tool, developed by Simpson (2005). For this vehicle model, the most fuel-efficient speed is around 32 mph. As shown in Figure 6, vehicles start to consume more energy per unit distance when their velocities are either above or below 32 mph. According to the result, the efficiency of the VSL algorithm proposed in this study varies in different scenarios. Percentages of energy consumption reduction from using VSL vary with market penetration of compliant vehicles, demand, and free flow speed.

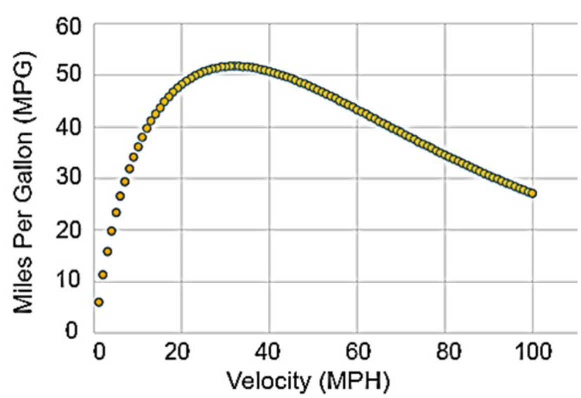

Figure. 6: Relationship between velocity and energy consumption.

5.3.1 Effects of VSL on stop-and-go conditions

Table 1 provides a sample scenario of how VSL impacts the velocities and number of vehicles for both compliant vehicles and non-compliant vehicles in a given network, using the results obtained by the simulation controlled by fixed speed limit (FSL) and variable speed limit (VSL). Column 2,3,5, and 6 are the occupancies of compliant vehicles and non-compliant vehicles in each cell. The simulation uses a free flow speed of 40 mph, and a backward shockwave speed of 20 mph. The structure of the network is shown in Figure 4, and all 4 signals follow the same 2-phase cycle in Figure 5 but with different offsets. There are six links in the test network. Every link has a length of 1 mile and 3 lanes with a capacity of 1200 veh per lane for a total capacity of 3600 vehicle per hour (vph). Four of them are modelled with cell transmission model (Link 23, 34, 45, 56) and tested using VSL algorithm. Link 12 and 67 are centroid connectors used to send vehicles to the test network and remove vehicles from the network. Table 1 shows cell occupancies and speed limits at $t = 1050$ sec of Link 34 with a demand of 1800 vph with 70% compliant vehicles.

Table 1: Cell occupancies for both variable speed limit and fixed speed limit for link 34 at time 1050.

	Variable Speed Limit (VSL)			Fixed Speed Limit (FSL)		
Cell ID	Occ (CV)	Occ (NCV)	VSL	Occ (CV)	Occ (NCV)	FSL
1	0.08	0	34	0	0	40
2	0.84	0	32	0	0	40
3	3.05	0	32	0	0	40
4	4.95	0.75	32	2.1	0.9	40
5	4.3	1.37	32	2.45	1.05	40
6	2.8	1.26	32	4.2	1.8	40
7	1.23	1.71	28	4.2	1.8	40
8	3.9	1.53	38	4.2	1.8	40
9	1.97	1.14	33	2.8	1.2	40
10	1.48	0	32	0	0	40
11	2.47	0	32	0	0	40
12	3.32	0	32	0	0	40
13	4.24	0.67	32	1.05	0.45	40
14	4.62	0.9	25	2.1	0.9	40
15	2.02	4.17	8	11.55	4.95	40

Table 1 proves that the proposed VSL algorithm can help mitigate the stop-and-go condition of vehicles in the test network. In Table 1, the current interval is a red light interval for Link 34. Cell 15 is the last cell of the link and is directly connected to the signalized intersection. Under the control of VSL, vehicle speeds are lower than 40 mph for each cell. The next green interval starts after 14 sec and ends after 47 sec from now, and the second green interval starts after 70 sec and ends after 103 sec from now. Vehicles in the first seven cells in this link do not have a chance to catch the next green light interval because they need a speed higher than 40 mph to catch next green light interval, while vehicles in the last eight cells can catch the next green light interval by reducing their speeds. The feasible ranges of speeds for Cells 2,3,4,10,11, and 13 include 32 mph, which is the most energy-efficient speed for the vehicle type used in this study, so speed limits for these cells are set to be 32 mph.

The occupancies of Cell 15 for VSL and FLS are 2.02 and 11.55. The number of the waiting vehicles with VSL is less than the number of waiting vehicles with FSL, because vehicles with VSL are set to pass through the green lights rather than waiting for the red lights. When the traffic light is red, VSLs reduce the speed limit of compliant vehicles and make fewer vehicles to approach and stop at the intersection. As compliant vehicles approach Cell 15, their velocities are reduced. As a result, fewer vehicles will move to the next cell and wait for the red light in Cell 15. More vehicles will enter Cell 15 when the light has already turned green. In Table 34, there is no effect of moving bottleneck on non-compliant vehicles because the flow rate of non-compliant vehicle flows does not exceed cell capacities. Therefore, the velocities of non-compliant vehicles stay the free flow speed of 40 mph.

5.3.2 Market penetration of compliant vehicles

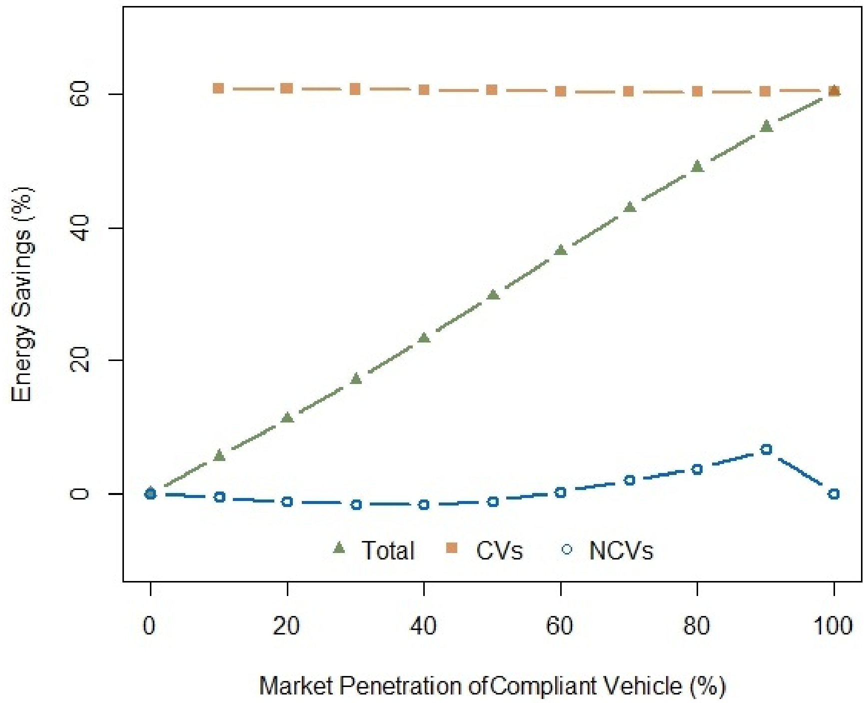

Figure. 7: The effects of market penetration of compliant vehicles on energy savings.

Results in Figure 7 use the same network as Figure 4, with a free flow speed of 40 mph. As shown in Figure 7, market penetration of compliant vehicles has no impact on their energy savings because they follow VSLs regardless of the velocities of other vehicles. For non-compliant vehicles, their percentages of energy savings are sometimes negative. Although moving bottleneck is intended to slow them down, non-compliant vehicles often attempt to overtake it. At the intersection, the moving bottleneck occupies the space of non-compliant vehicles and make them have low efficiency passing through the intersection, which leads to an increase in their energy consumption. For example, if the maximum flow rate at the intersection is 10 per time step, and there are 20 compliant vehicles and 5 non-compliant vehicles are going to pass through the intersection. Then most of the space will be taken by compliant vehicles with little remaining space for non-compliant vehicles. For percentages of overall energy saving, they are always positive and increase with the market penetration of compliant vehicles.

5.3.3 Demand

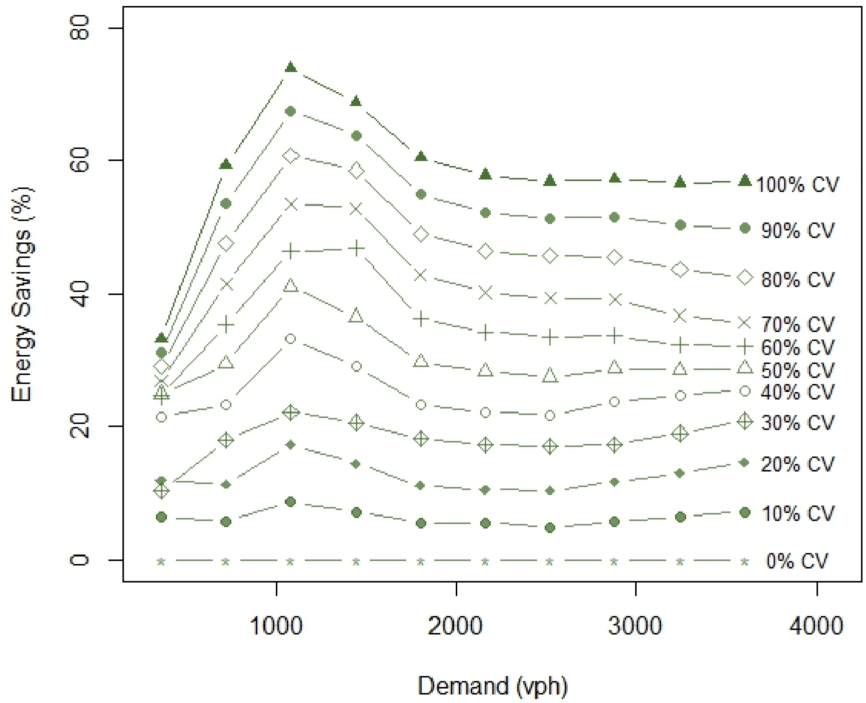

Figure. 8: The effects of demand on energy savings for different percentages of compliant vehicles.

Figure 8 is based on the same network as Figure 4, with variable demand from 360 vph to 3600 vph, and percentage of compliant vehicles varying from 0% to 100 %. As demand increases, energy savings first increase but later decrease after reaching 1080 vph. Queues form at the traffic signals because not all vehicles can pass through the green light before it turns red. Energy savings start to decrease when compliant vehicles behind the bottleneck are in a queue at jam density. As always, the percentage of energy savings increases with the percentage of compliant vehicles.

5.3.4 Free-flow speed

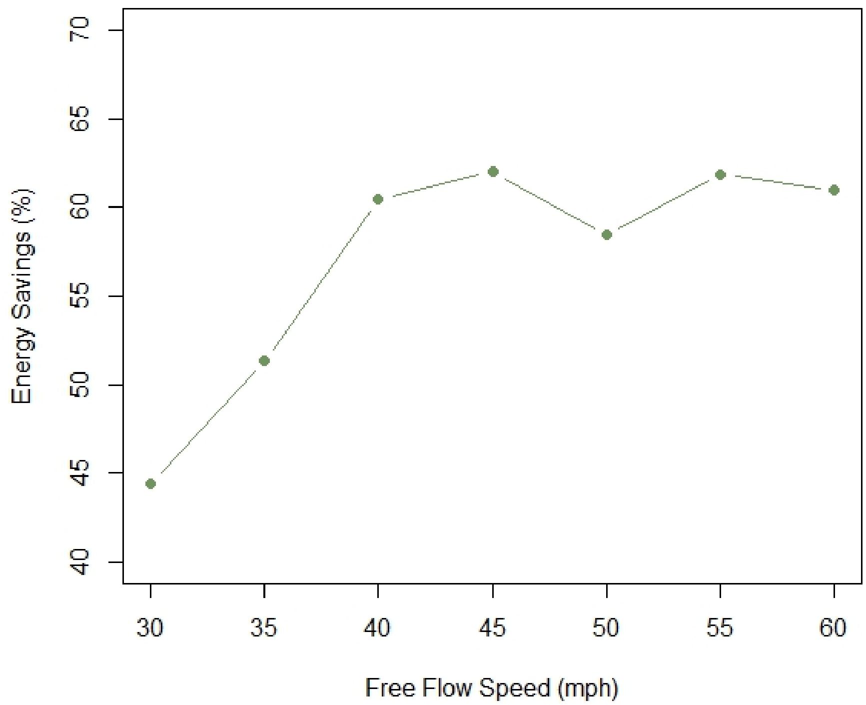

Figure. 9: The effects of free flow speed on energy savings.

Figure 9 is based on the same network as Figure 4 but with 100% compliant vehicles. On average, as free flow speed decreases, the percentage of energy reductions also decreases. The VSL algorithm in this study focuses on reducing velocities as appropriate, but since a lower free flow speed generally reduces energy consumption, VSL may have fewer impacts if the free flow speed is already low. On the other hand, as shown in Figure 9, vehicles start to consume more energy per distance travelled when velocities are below 32 mph. When VSL attempts to help vehicles avoid the red light and free flow speed is also low, sometimes the only option to avoid the red light is to have a low speed limit that may reduce energy efficiency and result in a smaller percentage of energy saving. Our algorithm will, however, not assign a very low velocity in order to avoid red lights but waste more energy than free flow speed.

5.3.5 Total System Travel Time

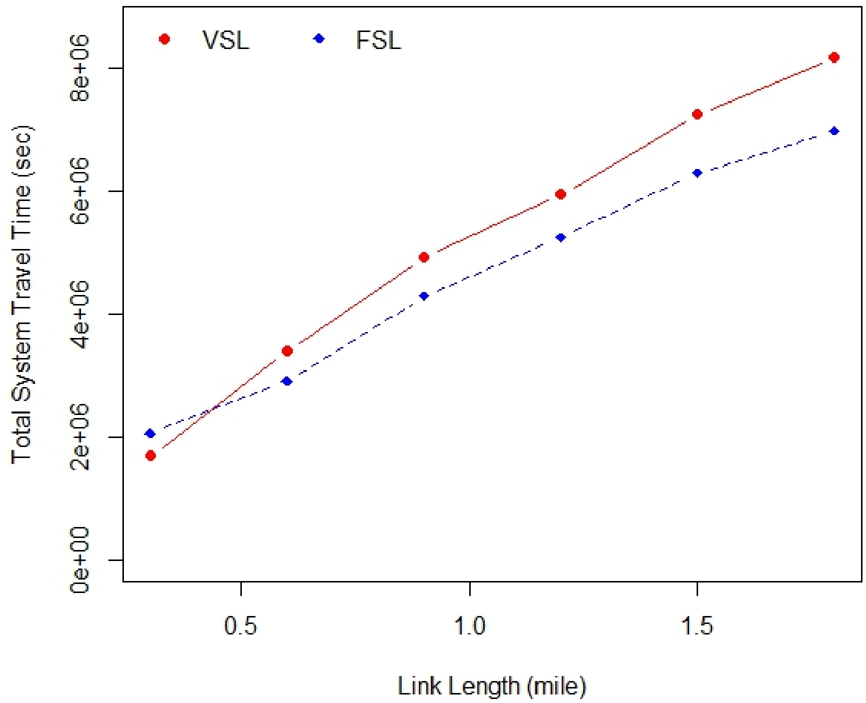

Figure. 10: Total system travel times with FSL and VSL

Figure 10 shows the change in the total system travel time with the average link length of the network. The simulation was run under a demand of 3600 veh per hour with 100% compliant vehicles. In Figure 10, the solid line represents VSL and the dashed line represents FSL. The total system travel time increases as the average link length of the network increases because it takes vehicles longer time to arrive the destination when paths become longer. The comparison between the total system travel time between the FSL and VSL reflects the effectiveness of the VSL control algorithm. The VSL control has smaller total system travel time than FSL when it is applied to short links with lengths smaller than 0.5 miles. When the link length becomes longer, vehicles under the control of VSL has larger travel time than vehicles under the control of FSL. The VSL algorithm proposed in this study is focused on reducing energy consumption and the delay at the intersection. The travel time of vehicles is composed of the link travel time and the intersection waiting time. The VSL algorithm leads to larger link travel time because it pushes vehicles to follow a calculated speed limit smaller than the fixed speed limit. When the link length is small, the reduction on the intersection waiting time is larger than the increase in the link travel time, so VSL has smaller total system travel time than FSL. As the link length gets longer, the reduction on the intersection cannot exceed the increase in the link travel time, so the total travel time of VSL becomes larger than FSL.

5.4 Discussion

Table 2: Input values for different scenarios

	link length (mile)	free-flow speed (mph)	demand (vph)	market penetration (%)
5.3.1	1	40	1080	70
5.3.2	1	40	1080	0-100 (+10)
5.3.3	1	40	360-3600 (+360)	0-100 (+10)
5.3.4	1	30-60 (+5)	1080	100
5.3.5	0.3-1.8 (+0.3)	40	3600	100

In this section, we used sensitivity analysis to explore the effects of traffic demand, market penetration, free-flow speed, and the link length on the energy consumption and the travel time. Table 2 shows the input values for these variables in different scenarios. In section 5.3.2, an increase in the market penetration improves the energy saving. In section 5.3.3, an increase in the demand under uncongested condition improves the energy saving. Under congested condition, an increase in the demand worsens the energy saving. In section 5.3.4, an increase in the free-flow speed improves the energy saving. In section 5.3.5, VSL has benefit in saving travel time compared with FSL when the link length is small. When the link length is large, there is no benefit in travel time using VSL.

6 Safety analysis

This section investigated the safety implication of a Cell Transmission Model (CTM) using Variable Speed Limit (VSL) strategies to reduce fuel consumption at various Connected Vehicle (CAV) market penetrations on a simple arterial corridor with traffic signals. We implemented the CTM based on a kinematic wave theory and conducted simulations with various scenarios based on different free-flow speeds, traffic demands, and CAV market penetrations. Shockwave occurrence was used as an indicator to evaluate the likelihood of crash occurrence in this study. This task analysed the safety implication of a transportation network with a mix of CV operated under VSL strategies with objectives to reduce energy consumption in a CTM based simulation environment.

6.1 Methodology

The same network as illustrated in Figure 4 was used for safety analysis. There were 45 traffic scenarios based on 3 different free-flow speeds (30, 40, and 50 mph), 3 traffic demands (1080, 2400, and 3600 vph), and 5 different CAV market penetrations (CAV 0, CAV 0.3, CAV 0.5, CAV 0.7, and CAV 1) were simulated using a simulation time step of 6 seconds. For example, CAV 0.7 includes 70% of autonomous vehicles and 30% of vehicles driven by human drivers. Shockwave speed, as described in Eq. 34, at each simulation step was computed based on the flow rate and density differences between two adjacent cells. Shockwave occurrence for each simulation scenario was analysed and compared with different CV market penetrations.

$$v_s = \frac{q(t,x) - q(t,x-1)}{k(t,x) - k(t,x-1)} \tag{34}$$

In equation (34), $v_s(t,x)$ is the shockwave speed at time step t and cell x, $k(t,x)$ and $q(t,x)$ are the traffic density and flow at cell x and time t, and $k(t,x-1)$ and $q(t,x-1)$ are the traffic density and flow at cell $x-1$ and time t respectively.

6.2 Analysis results

6.2.1 Shockwave occurrence

Lee and Volpatti (2010) indicated that crashes are more likely to occur when the forward shockwave speed is lower. We first examined the occurrence rate of forward shockwave (0-10 mph) with different free-flow speeds (30, 40 and 50 mph) and traffic demands (1080, 2400, and 3600 vehicles per hour). Figure 11 - Figure 13 display the low forward shockwave occurrence rate for 5 different CV market penetration rates, respectively. The standard deviation of forward shockwave occurrence decreases as the CV market penetration rate increases for medium and high traffic demands (2400 & 3600 vph). When the traffic demand is relatively low (1080 vph), the forward shockwave occurrence rate increases from 70 to 100% CV market penetration for scenarios with free-flow speed at 40 and 50 mph (Blue/bottom lines in Figure 12 and 13).

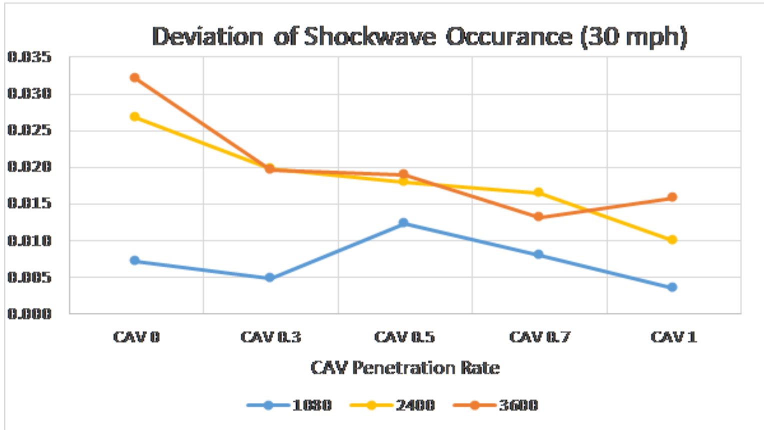

Figure. 11: Deviation of Low Forward Shockwave Occurrence at Free-Flow Speed 30 mph

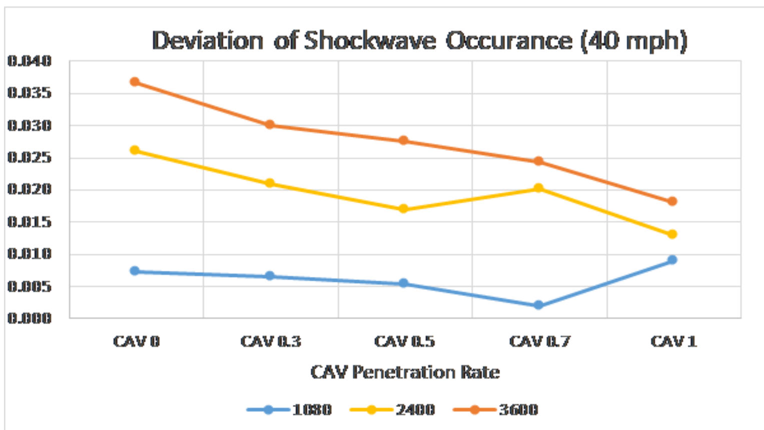

Figure. 12: Deviation of Low Forward Shockwave Occurrence at Free-Flow Speed 40 mph

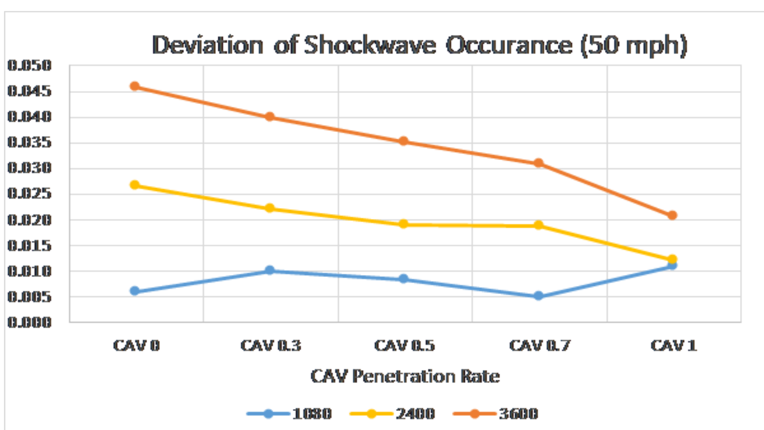

Figure. 13: Deviation of Low Forward Shockwave Occurrence at Free-Flow Speed 50 mph

Similarly, we also examined the backward shockwave (< 0 mph) occurrence rate with different free-flow speeds and traffic demands. Figure 14 - 16 display the backward shockwave occurrence rate for 5 different CV market penetration rates, respectively. Overall, the standard deviation of backward shockwave occurrence decreases as the CV market penetration rate increases. At 30% CV market penetration rate in Figure 14, backward shockwave occurrence rates for all low, medium, and high traffic demands have a relative low deviation of 0.01 as compared to the other CV penetrations for simulation scenarios with free-flow speed of 30 mph. Simulation scenarios with CV have lower shockwave deviation than the scenarios without CV. On average, the shockwave deviation in traffic with CV (CAV0.3, CAV0.5, CAV0.7 & CAV1) controlled by VSL is over 55% lower than the deviation from traffic with non-VSL compliant vehicles (i.e., CAV0, vehicles human drivers).

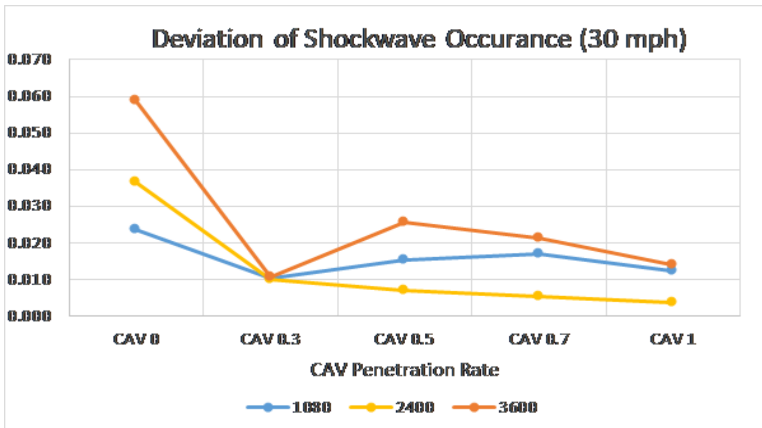

Figure. 14: Deviation of Backward Shockwave Occurrence at Free-Flow Speed 30 mph

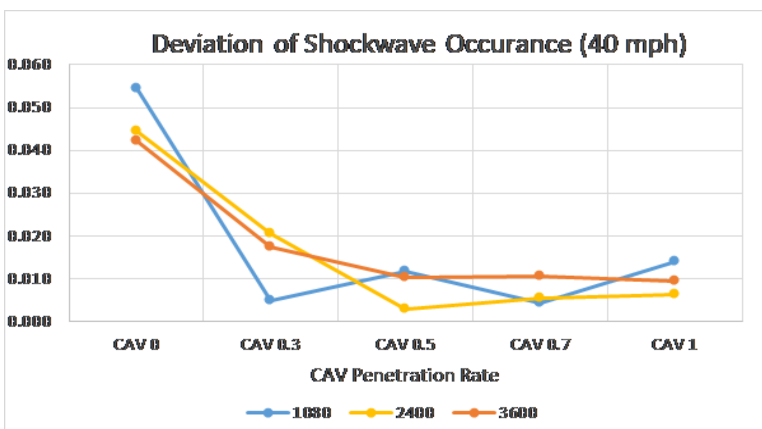

Figure. 15: Deviation of Backward Shockwave Occurrence at Free-Flow Speed 40 mph

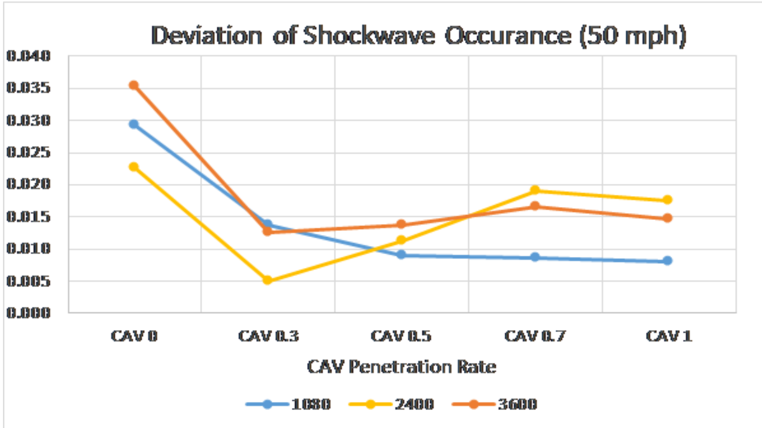

Figure. 16: Deviation of Backward Shockwave Occurrence at Free-Flow Speed 50 mph

6.2.2 Travel time

Allaby et al. (2007) indicated that the implementation of VSLs could improve safety at a cost of increased travel times on a congested highway. The research team analysed the impact of VSL strategies on roadway with various CAV market penetrations. Figure 17 displays the average travel time for 3 different traffic demands (1080, 2400, and 3600 vph) and 5 different CV market penetrations at a free-flow speed of 30 mph. On average, the Travel Times (TT) for traffic scenarios with 100% CAV are respectively 22%, 29%, and 15% longer than the TT of traffic scenarios with vehicles 100% operated by human.

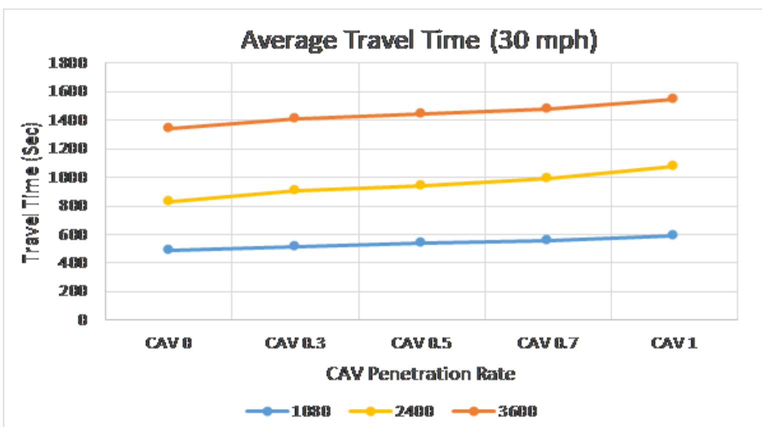

Figure. 17: Average Travel Time for Different Traffic Demands and CV Market Penetrations at Free-Flow Speed of 30 mph.

Similarly, Figure 18 displays the average travel time for 3 different traffic demands (1080, 2400, and 3600 vph) and 5 different CV market penetrations at a free-flow speed of 40 mph. The average TT for traffic scenarios with 100% CAV are respectively 23%, 32%, and 14% longer than the TT of traffic scenarios with vehicles 100% operated by human at 40 mph. For fixed speed limit simulation runs, the average travel times were about 700, 1100, and 1200 for demands of 1080, 2400, and 3600 vph, respectively. We believe, the large increase in the travel time results from the increase in the congestion at the signalized intersections.

Figure 19 displays the average travel time for 3 different traffic demands (1080, 2400, and 3600 vph) and 5 different CV market penetrations at a free-flow speed of 50 mph. The average TT for traffic scenarios with 100% CAV are respectively 32%, 35%, and 16% longer than the TT of traffic scenarios with vehicles 100% operated by human at 50 mph.

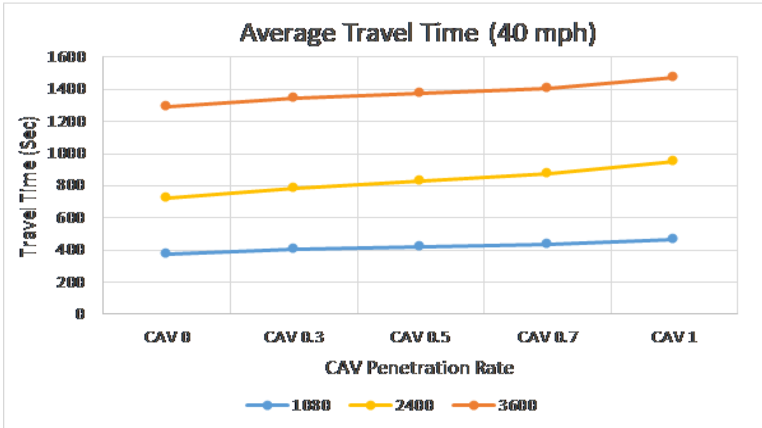

Figure. 18: Average Travel Time for Different Traffic Demands and CV Market Penetrations at Free-Flow Speed of 40 mph.

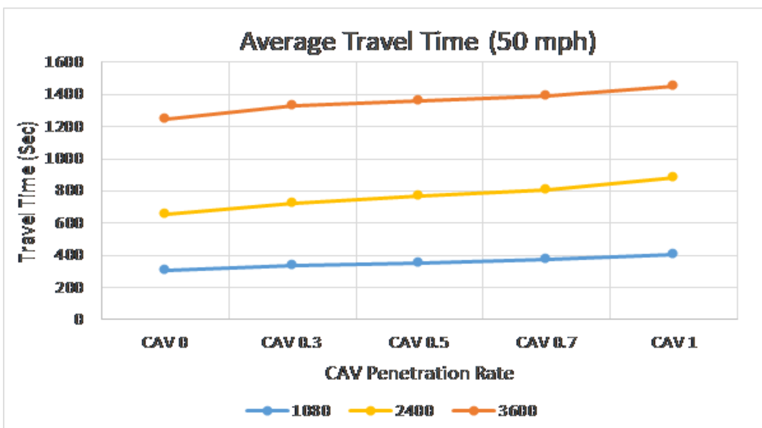

Figure. 19: Average Travel Time for Different Traffic Demands and CV Market Penetrations at Free-Flow Speed of 50 mph.

Table 3 summarized the percentage of travel time increases by different free-flow speeds and traffic demands. For traffic demand at 1080 vph, the average travel time increases from 0% (all vehicles driven by human operators) to 100% CAV market penetrations by 22.1%, 23.4%, and 32% for free-flow speed at 30, 40 and 50 mph, respectively. When the traffic demand is relatively low (i.e., 1080 vph), the average increase of TT of a network with 100% CAV will be significantly longer (9.9%) than the scenarios with higher traffic demand at 3600 vph (1.1%).

6.3 Discussion

We investigated the safety implication of applying Variable Speed Limit (VSL) strategies in a Cell Transmission Model (CTM) based simulation model with a goal to reduce fuel consumption. Various simulation

Table 3: Percentage of Travel Time Increase by Traffic Demand and Free-Flow Speed

Travel Time Increase (%)		**30 mph**	**40 mph**	**50 mph**	**% change (30 to 50 mph)**
Traffic Demand	**1080 vph**	22.1%	23.4%	32.0%	9.9%
	2400 vph	29.3%	32.0%	35.2%	5.9%
	3600 vph	14.9%	14.4%	16.1%	1.1%

scenarios with 3 different traffic demands (1080, 2400 and 3600 vph) and 5 market penetration rates (0%, 30%, 50%, 70%, and 100%) of Autonomous Vehicle (AV) were studied along a simple arterial corridor with 5 signalized intersections. A 6-sec simulation time step and a cell size of 30 in each link were implemented in the simulation model. The sudden change of traffic flow can generate discontinuities in the traffic stream in the form of kinematic shockwaves. Shockwave occurrence was used as an indicator to evaluate the likelihood of crash occurrence in the study. In general, the standard deviation of backward shockwave occurrence decreases as the CAV market penetration rate increases. Simulation scenarios with CV have lower shockwave deviation than the scenarios with all vehicles operated by human drivers. On average, the shockwave deviation in traffic scenario with autonomous vehicles (CAV0.3, CAV0.5, CAV0.7 & CAV1) and controlled by VSL is over 55% lower than the deviation from scenarios with non-VSL compliant vehicles (i.e., CAV0, vehicles operated by human drivers). The simulation results indicated that applying VSL strategy on an arterial network with higher percentage of autonomous vehicles will likely increase the average vehicle travel time. The increase of travel time becomes higher for a traffic network with a relatively higher free-flow speed. For example, at traffic demand of 2400 vph, the average travel time increases from CAV0 (all vehicles driven by human operators) to CAV1 (fully autonomous vehicles) by 29%, 32%, and 35% for free-flow speed at 30, 40 and 50 mph, respectively. Similarly, for traffic demand at 3600 vph, the average travel time increases from CAV0 to CAV1 by 15%, 14%, and 16% for free-flow speed of 30, 40 and 50 mph, respectively. Applying VSL strategy in a CAV traffic flow is likely to increase the average travel time in a network. However, a traffic flow with increasing percentage of autonomous vehicles will reduce the shockwave deviations from our simulation results. Our results indicated that VSL with higher number of CAV in a network can help harmonize traffic conditions to faster damp out shockwaves and thus reduce the likelihood of crash occurrence.

7 Conclusions

Variable speed limits (VSL) can be better implemented with the help of connected/autonomous vehicles (CAVs), as these vehicles can communicate with infrastructure at intersections and can always follow the speed limit. These vehicles can also serve as a moving bottleneck and force other vehicles to reduce speed. To model the effect of VSL on the traffic condition, the cell transmission model was modified to model the interaction between compliant vehicles that always follow the VSLs and non-compliant vehicles that try to pass the moving bottleneck created by compliant vehicles. Simulation was conducted with a test network with six links to explore the effect of VSL on energy consumption under multiple scenarios. After the simulation, the safety and energy consumption effects of VSL were analyzed. The simulation results showed that VSL has a significant improvement on the energy consumption of the test network and the effect of VSL is influenced by market penetration of autonomous vehicles, demand, and free flow speed.

1. When the demand is 1800 vehicles per hour, the percentage of total energy savings increases as the market penetration of compliant vehicles increases. The VSL reduces the energy consumption of compliant vehicles by 60% but sometimes leads to more energy consumption for non-compliant vehicles.

2. The percentage of total energy savings increases when the demand increases from 0 to 360 vehicles per hour per lane, and then decreases as the demand increases from 360 to 1200 vehicles per hour per lane.

3. When the demand is 1800 vehicles per hour and the market penetration of CAVs is 100%, the percentage of total energy saving increases as the free flow speed increases from 30 mph to 45 mph and stays at 68% when the free flow speed is between 45 and 60 mph.

4. When the demand is 3600 vehicles per hour and the market penetration of CAVs is 100%, the total system travel time increases as the average link length increases. When the average link length is smaller than 0.5 miles, the network controlled by VSL has a smaller total system travel time than the network controlled by FSL.

5. As the market penetration rate of CAV increases in a network with VSL, the deviance of shockwave occurrence decreases. VSL with a higher number of CAV in a network can help harmonize traffic conditions to damp out shockwaves.

A small test network was used in this project. The largest percentage of energy saving is 74% with a demand of 360 vehicles per hour per lane and 100% CAVs. This value of energy saving results from the high energy saving at the intersection. When the length of each link is increased from 1 mile to 3 miles, the percentage of energy savings drops to 68%. To implement the VSL strategy in a real network, this algorithm needs to be tested on a larger network. As the values of speed and acceleration used to calculate the energy assumption are average values for all vehicles in the same cell, the percentage of energy saving calculated by CTM may be biased. Therefore, the result of CTM should be compared with the result of a microscopic simulation model. The VSL control algorithm designed in this study may not find the optimal VSLs, so other algorithms can be explored (although the problem appears to be a non-convex quadratic program).

References

Abdel-Aty, M., Dilmore, J., and Dhindsa, A. (2006). Evaluation of variable speed limits for real-time freeway safety improvement. *Accident Analysis & Prevention*, 38(2):335–345.

Ahmed, M. M., Abdel-Aty, M., and Yu, R. (2012). Bayesian updating approach for real-time safety evaluation with automatic vehicle identification data. *Transportation Research Record*, 2280(1):60–67.

Allaby, P., Hellinga, B., and Bullock, M. (2007). Variable speed limits: Safety and operational impacts of a candidate control strategy for freeway applications. *IEEE Transactions on Intelligent Transportation Systems*, 8(4):671–680.

Asadi, B. and Vahidi, A. (2011). Predictive cruise control: Utilizing upcoming traffic signal information for improving fuel economy and reducing trip time. *IEEE transactions on control systems technology*, 19(3):707–714.

Astarita, V., Festa, D. C., Giofrè, V. P., and Guido, G. (2019). Surrogate safety measures from traffic simulation models a comparison of different models for intersection safety evaluation. *Transportation research procedia*, 37:219–226.

Bachmann, C., Roorda, M., and Abdulhai, B. (2011). Improved time-to-collision definition for simulating traffic conflicts on truck-only infrastructure. *Transportation Research Record: Journal of the Transportation Research Board*, (2237):31–40.

Barth, M., Mandava, S., Boriboonsomsin, K., and Xia, H. (2011). Dynamic eco-driving for arterial corridors. In *Integrated and Sustainable Transportation System (FISTS), 2011 IEEE Forum on*, pages 182–188. IEEE.

Breton, P., Hegyi, A., De Schutter, B., and Hellendoorn, H. (2002). Shock wave elimination/reduction by optimal coordination of variable speed limits. In *Intelligent Transportation Systems, 2002. Proceedings. The IEEE 5th International Conference on*, pages 225–230. IEEE.

Chambers, A., Pande, A., and Bertini, R. L. (2017). Empirical before and after evaluation of a variable speed limit system from a safety management perspective. In *TRB 96th Annual Meeting, Washington DC*.

Charly, A. and Mathew, T. V. (2017). Estimation of modified time to collision as surrogate for mid-block crashes under mixed traffic conditions. In *TRB 96th Annual Meeting, Washington DC*.

Cho, H. and Kim, Y. (2012). Analysis of traffic flow with variable speed limit on highways. *KSCE Journal of Civil Engineering*, 16(6):1048–1056.

Conran, C. and Abbas, M. (2018). Modeling driver behavior under variable speed limits. In *TRB 97th Annual Meeting, Washington DC*.

Courant, R., Friedrichs, K., and Lewy, H. (1967). On the partial difference equations of mathematical physics. *IBM Journal of Research and Development*, 11(2):215–234.

Daganzo, C. F. (1994). The cell transmission model: A dynamic representation of highway traffic consistent with the hydrodynamic theory. *Transportation Research Part B: Methodological*, 28(4):269–287.

Daganzo, C. F. (1995). The cell transmission model, part ii: network traffic. *Transportation Research Part B: Methodological*, 29(2):79–93.

Daganzo, C. F. and Laval, J. A. (2005). Moving bottlenecks: A numerical method that converges in flows. *Transportation Research Part B: Methodological*, 39(9):855–863.

Downey, M. B. (2015). Evaluating the effects of a congestion and weather responsive advisory variable speed limit system in Portland, Oregon.

Godunov, S. K. (1959). A difference method for numerical calculation of discontinuous solutions of the equations of hydrodynamics. *Matematicheskii Sbornik*, 89(3):271–306.

Gousios, S., Garber, N., and Liu, Q. (2009). *Simulation based validation of time to collision as a safety performance surrogate*, volume 107. WIT Press.

Hadiuzzaman, M. and Qiu, T. Z. (2013). Cell transmission model based variable speed limit control for freeways. *Canadian Journal of Civil Engineering*, 40(1):46–56.

He, X., Liu, H. X., and Liu, X. (2015). Optimal vehicle speed trajectory on a signalized arterial with consideration of queue. *Transportation Research Part C: Emerging Technologies*, 61:106–120.

He, Z., Zheng, L., Song, L., and Zhu, N. (2017). A jam-absorption driving strategy for mitigating traffic oscillations. *IEEE Transactions on Intelligent Transportation Systems*, 18(4):802–813.

Hegyi, A., De Schutter, B., and Heelendoorn, J. (2003). Mpc-based optimal coordination of variable speed limits to suppress shock waves in freeway traffic. In *American Control Conference, 2003. Proceedings of the 2003*, volume 5, pages 4083–4088. IEEE.

Hegyi, A., De Schutter, B., and Hellendoorn, H. (2005a). Model predictive control for optimal coordination of ramp metering and variable speed limits. *Transportation Research Part C: Emerging Technologies*, 13(3):185–209.

Hegyi, A., De Schutter, B., and Hellendoorn, J. (2005b). Optimal coordination of variable speed limits to suppress shock waves. *IEEE Transactions on intelligent transportation systems*, 6(1):102–112.

Hellinga, B. and Mandelzys, M. (2011). Impact of driver compliance on the safety and operational impacts of freeway variable speed limit systems. *Journal of Transportation Engineering*, 137(4):260–268.

Hou, J., List, G. F., and Guo, X. (2014). New algorithms for computing the time-to-collision in freeway traffic simulation models. *Computational intelligence and neuroscience*, 2014:57.

Khondaker, B. and Kattan, L. (2015). Variable speed limit: an overview. *Transportation Letters*, 7(5):264–278.

Kress, D., Bertini, R. L., and Bogenberger, K. (2018). Implementations of variable speed limit systems: A worldwide overview. In *TRB 97th Annual Meeting, Washington DC.*

Kwon, E., Brannan, D., Shouman, K., Isackson, C., and Arseneau, B. (2007). Development and field evaluation of variable advisory speed limit system for work zones. *Transportation Research Record: Journal of the Transportation Research Board*, (2015):12–18.

Lee, C., Hellinga, B., and Saccomanno, F. (2006). Evaluation of variable speed limits to improve traffic safety. *Transportation Research Part C: Emerging Technologies*, 14(3):213–228.

Lee, C. and Volpatti, S. (2010). Effects of shock waves on freeway crash likelihood. *Open Transportation Journal*, 4:61–70.

Levin, M., Duell, M., and Waller, S. (2014). Effect of road grade on networkwide vehicle energy consumption and ecorouting. *Transportation Research Record: Journal of the Transportation Research Board*, (2427):26–33.

Lighthill, M. J. and Whitham, G. B. (1955). On kinematic waves. ii. a theory of traffic flow on long crowded roads. In *Proceedings of the Royal Society of London A: Mathematical, Physical and Engineering Sciences*, volume 229, pages 317–345. The Royal Society.

Martinez, I. and Jin, W.-L. (2018). Optimal location of variable speed limit application area. In *TRB 97th Annual Meeting, Washington DC.*

Mudgal, A. and Hourdos, J. (2017). Impact of variable speed limits on freeway rear-end collisions.

Nissan, A. (2010). *Evaluation of variable speed limits: Empirical evidence and simulation analysis of stockholm's motorway control system.* PhD thesis, KTH.

Pande, A. and Abdel-Aty, M. (2006). Comprehensive analysis of the relationship between real-time traffic surveillance data and rear-end crashes on freeways. *Transportation research record*, 1953(1):31–40.

Qi, X., Wang, L., Zhang, F., and Ma, W. (2019). Analysis the impact of a freeway speed harmonization system using connected vehicles: Case study of field test in seattle. TRB 98th Annual Meeting, Washington DC.

Qu, X., Wang, W., Ran, B., and Dai, Y. (2017). Quantitative analysis of the impact of variable speed limits on motorway safety. In *TRB 96th Annual Meeting, Washington DC,*.

Richards, P. I. (1956). Shock waves on the highway. *Operations Research*, 4(1):42–51.

Sanchez, M., Cano, J.-c., and Kim, D. (2006). Predicting traffic lights to improve urban traffic fuel consumption. In *ITS Telecommunications Proceedings, 2006 6th International Conference on*, pages 331–336. IEEE.

Simoni, M. D. and Claudel, C. G. (2017). A fast simulation algorithm for multiple moving bottlenecks and applications in urban freight traffic management. *Transportation Research Part B: Methodological*, 104:238–255.

Simpson, A. G. (2005). Parametric modelling of energy consumption in road vehicles.

Talebpour, A., Mahmassani, H., and Hamdar, S. (2013). Speed harmonization: Evaluation of effectiveness under congested conditions. *Transportation Research Record: Journal of the Transportation Research Board*, (2391):69–79.

Ubiergo, G. A. and Jin, W. (2016). Mobility and environment improvement of signalized networks through vehicle-to-infrastructure (v2i) communications. *Transportation Research Part C: Emerging Technologies*, 68:70–82.

van Driel, C. (2007). Driver support in congestion. an assessment of user needs and impacts on driver and traffic flow.

Wasson, J., Boruff, G., Hainen, A., Remias, S., Hulme, E., Farnsworth, G., and Bullock, D. (2011). Evaluation of spatial and temporal speed limit compliance in highway work zones. *Transportation Research Record: Journal of the Transportation Research Board*, (2258):1–15.

Yang, H., Ozbay, K., and Bartin, B. (2010). Application of simulation-based traffic conflict analysis for highway safety evaluation. *Proceedings of the 12th WCTR, Lisbon, Portugal*.

Yu, R. and Abdel-Aty, M. (2013). Utilizing support vector machine in real-time crash risk evaluation. *Accident Analysis & Prevention*, 51:252–259.

Zhu, F. and Ukkusuri, S. V. (2018). Modeling the proactive driving behavior of connected vehicles: A cell-based simulation approach. *Computer-Aided Civil and Infrastructure Engineering*, 33(4):262–281.

Ziliaskopoulos, A. K. (2000). A linear programming model for the single destination system optimum dynamic traffic assignment problem. *Transportation Science*, 34(1):37–49.